DARPA/ONR Grant #N00014-91-J-1976

Eighth Quarterly Progress Report
(covering the period of 05/01/93 - 07/31/93)

Project Title: Development of Ultra-Low Noise, High Performance III-V Quantum Well Infrared Photodetectors (QWIPs) for Focal Plane Array Staring Image Sensor Systems

Submitted to

Max N. Yoder

Office of Naval Research
Code 3140
800 North Quincy Street
Arlington, VA 22217-5000

Prepared by

Sheng S. Li
Professor

Dept. of Electrical Engineering
University of Florida
Gainesville, Florida 32611

Tel.(904)-392-4937
Fax(904)-392-8671
E-Mail: ShengLi@ENG.UFL.EDU

August 1, 1993

DARPA/ONR Grant #N00014-91-J-1976

Eighth Quarterly Progress Report
(covering the period of 05/01/93 - 07/31/93)

Project Title: Development of Ultra-Low Noise, High Performance III-V Quantum Well Infrared Photodetectors (QWIPs) for Focal Plane Array Staring Image Sensor Systems

Submitted to

Max N. Yoder

Office of Naval Research
Code 3140
800 North Quincy Street
Arlington, VA 22217-5000

Prepared by

Sheng S. Li
Professor

Dept. of Electrical Engineering
University of Florida
Gainesville, Florida 32611

Tel.(904)-392-4937
Fax(904)-392-8671
E-Mail: ShengLi@ENG.UFL.EDU

August 1, 1993

REPORT DOCUMENTATION PAGE

Form Approved
OMB No. 0704-0188

1. AGENCY USE ONLY (Leave blank)	2. REPORT DATE	3. REPORT TYPE AND DATES COVERED
	August 1, 1993	Quarterly Progress Report:5/1--7/31/93

4. TITLE AND SUBTITLE
Development of Ultra-low Dark Current, High Sensitivity Planar Metal Grating Coupled III-V Quantum Well Infrared Photodetectors for Focal Plane Array Staring IR Sensor Systems

5. FUNDING NUMBERS
ONR G-N00014-91-J-1976

6. AUTHOR(S)
Sheng S. Li, Professor

7. PERFORMING ORGANIZATION NAME(S) AND ADDRESS(ES)
University of Florida
Gainesville, FL 32611

8. PERFORMING ORGANIZATION REPORT NUMBER
92122803

9. SPONSORING/MONITORING AGENCY NAME(S) AND ADDRESS(ES)
US Navy, Office of Naval Research
800 North Quincy Street, Code 1512B-SM
Arlington, VA 22217-5000

10. SPONSORING/MONITORING AGENCY REPORT NUMBER

11. SUPPLEMENTARY NOTES

12a. DISTRIBUTION/AVAILABILITY STATEMENT
Approved for public release, distribution unlimited.

12b. DISTRIBUTION CODE

13. ABSTRACT *(Maximum 200 words)*

During this reporting period (05-01-93 to 07-31-93) we have continued to make excellent progress towards the program goals. We have made a major breakthrough in the development of a new normal incidence p-type strained layer InGaAs/InAlAs QWIP grown on InP by MBE, which achieved both the **lowest dark current** and **highest detectivity** ever reported for a QWIP operating at **8.1 um** and **77 K.** The device dark current at 77 K is one to two orders of magnitude smaller than its 300 K background photocurrent, which shows that this p-type strained layer QWIP is under BLIP operation at 77 K. Other tasks performed during this period include: (i) measured and compared the device dark current with 300 K background limited photocurrent (BLIP) for several QWIPs fabricated from GaAs/AlGaAs, InGaAs/InAlAs, and AlAs/AlGaAs material systems, (ii) designed a broad band 2-D square mesh grating coupler for the dual-mode operation GaAs QWIP to enhance the coupling quantum efficiency and responsivity of this QWIP in the 3-5 and 8-12 um bands, (iii) using a 2-D square mesh grating coupler to achieve maximum responsivity for an InGaAs SBTM QWIP, and (iv) performed noise characterization on four different types of III-V QWIPs and identified their noise sources. Detailed results and accomplishments are discussed in this report.

14. SUBJECT TERMS Quantum well infrared photodetectors (QWIPs), GaAs/AlGaAs, strained p-type, InGaAs/InAlAs, miniband transport, intersubband absorption, dark current, responsivity, detectivity, square mesh metal grating coupler.

15. NUMBER OF PAGES
62

16. PRICE CODE

17. SECURITY CLASSIFICATION OF REPORT	18. SECURITY CLASSIFICATION OF THIS PAGE	19. SECURITY CLASSIFICATION OF ABSTRACT	20. LIMITATION OF ABSTRACT
Unclassified.			Unlimited.

8th Quarterly Progress Report (05/1/93 - 07/31/93)

Project Title: Development of Ultra-low Dark Current, High Performance III-V Quantum Well Infrared Photodetectors (QWIPs) for Focal Plane Arrays Staring Imaging Sensor Systems.

Program Manager: Max N. Yoder, Office of Naval Research, Code 3140, Arlington, VA.

Principal Investigator: Sheng S. Li, Professor, University of Florida, Gainesville, FL.

Project Objectives:

1. To develop ultra-low dark current and high detectivity planar metal grating coupled bound-to-miniband (BTM) III-V quantum well infrared photodetectors (QWIPs) for 8 to 12 μm focal plane arrays (FPAs) staring IR sensor systems.

2. To develop novel type-I and type-II III-V QWIPs with single, multicolor, broad and narrow band spectral responses in the 8 to 14μm wavelength range. The material systems to be studied include n-type GaAs/AlGaAs, AlAs/AlGaAs, InGaP/GaAs grown on GaAs substrates, n-type and p-type strained layer InAlAs/InGaAs grown on InP substrate.

3. To conduct theoretical and experimental studies of the planar metal grating coupled structures for normal incidence illumination on QWIPs. Different metal grating coupled structures using 2-D square mesh and dot metal gratings will be studied in order to achieve high coupling quantum efficiency under normal frontside or backside illuminations on QWIPs.

4. To perform theoretical and experimental studies of dark current, photocurrent, noise optical absorption, spectral responsivity and detectivity for different types of QWIPs developed under this program.

I. Introduction

During this reporting period (05-01-93 to 07-31-93) we have continued to make excellent progress towards the program goals. We have designed, fabricated, and characterized a new **BLIP limited** normal incidence p-type strained layer InGaAs/InAlAs QWIP formed on the InP substrate, which achieved simultaneously the **lowest dark current and highest detectivity** ever reported for a QWIP operating at 77 K. The device dark current for this QWIP operating at 77 K is one to two orders of magnitude smaller than the 300 K background photocurrent, which shows that this p-type strained QWIP is under **BLIP** condition at 77 K. Specific tasks performed during this period include: (i) design, growth, fabrication, and characterization of a novel ultra-low dark current normal incidence p-type strained InGaAs/InAlAs QWIP grown on a semi-insulating InP substrate by the MBE technique, (ii) design, growth, and fabrication of a new multi-color enhanced bound-to-continuum band (EBTC) and bound-to-miniband (BTM) transition GaAs/GaInP QWIPs grown on GaAs substrate by the MOCVD technique, (iii) measured and compared the dark current and 300 K BLIP photocurrent for several QWIPs fabricated from GaAs/AlGaAs, InGaAs/InAlAs, and AlAs/AlGaAs material systems, (iv) designed a broad band 2-D square mesh grating coupler structure for a dual-mode operation GaAs QWIP to enhance the coupling quantum efficiency and to improve the responsivity and detectivity of this QWIP, (v) designed and fabricated a 2D square mesh grating coupler for the InGaAs SBTM QWIP for responsivity enhancement, (vi) completed noise characterization on four different types of III-V QWIPs and identified the noise sources in these QWIPs. Detailed accomplishments and publications are described in Section II. The technical results are presented in Section III.

II. Research Accomplishments and Publications

Research accomplishments and publications during this period are summarized as follows:

2.1 Research Accomplishments:

1. A new **BLIP** normal incidence p-type strained (PSL) InGaAs/InAlAs QWIP with peak response wavelength at $\lambda_p = 8.1\ \mu m$ and operating at 77 K has been developed for the first time. The BLIP detectivity for this QWIP at peak wavelength was found to be $5.9 \times 10^{10}\ cm - Hz^{1/2}/W$, at V_b = -2 V and T = 77 K. This is the highest value ever reported for a QWIP. The extremely low dark current observed in this QWIP at 77 K offers an excellent opportunity to fabricate high performance focal plane arrays using PSL-QWIPs for 77 K operation. Detailed

results for this QWIP are depicted in Section 3.1.

2. A comparison of the measured dark current and 300 K background photocurrent for four different QWIPs is depicted in Section 3.2. These QWIPs were grown by the MBE technique using GaAs/AlGaAs and AlAs/AlGaAs and InGaAs/InAlAs material systems. The results showed that two of these QWIPs offer background limited performance (BLIP) at 77 K.

3. Design, fabrication, and characterization of a broad band 2-D square mesh grating coupler formed on a dual-mode (DM) operation GaAs QWIP have been carried out. A flat coupling quantum efficiency of $\eta \sim 18\%$ was obtained for this QWIP under normal incidence backside illumination over the wavelength bands of $\lambda_p = 6 - 8 and 10 - 13 \mu$m. Detailed results are discussed in Section 3.3.

4. Enhancement of the coupling quantum efficiency for a grating coupled InGaAs SBTM QWIP has been realized using the 2-D square mesh metal grating coupler with different grating periods and grating aperture sizes. Detailed results are depicted in Section 3.4.

5. Completed noise characterization on four different types of III-V QWIPs. From the measurements of noise current as a function of frequency (10 to 10^5 Hzs), the noise sources in these QWIPs were identified. The results revealed that Johnson noise dominated in the PV mode operation QWIP while generation-recombination noise (g-r) noise prevailed in the PC mode operation QWIPs. Results of noise measurements on these QWIPs are discussed in Section 3.5.

6. Since the beginning of this project, one Ph.D. and three M.S. students have completed their degree working on the QWIP project sponsored by the ARPA/ONR. Two more Ph.D. students are in their final stage of research and are expected to graduate by Summer term, 1994. An AASERT sponsored Ph.D. student has started this summer working on the new high performance p-type strained layer InGaAs/InAlAs QWIPs for focal plane arrays applications.

2.2. Refereed Journal Papers:

1. L. S. Yu and S. S. Li,"A Low Dark Current, High Detectivity Grating Coupled AlGaAs/GaAs Mulitple Quantum Well IR Detector Using Bound-to-Miniband Transition for 10 μm Detection,"Appl. Phys. Letts., 59 (11), p.1332, Sept.9, 1991.

2. L. S. Yu, S. S. Li, and Pin Ho "Largely Enhanced Bound-to-Miniband Absorption in an InGaAs Multiple Quantum Well with a Short-Period Superlattice InAlAs/InGaAs Barrier " Applied Phys. Letts., 59 (21), p.2712, Nov. 18, 1991.

3. L. S. Yu, Y. H. Wang, S. S. Li and Pin Ho,"A Low Dark Current Step-Bound-to-Miniband Transition InGaAs/GaAs/AlGaAs Multiquantum Well Infrared Detector," Appl. Phys. Letts., 60(8), p.992, Feb.24, 1992.

4. L. S. Yu, S. S. Li,and P. Ho,"A Normal Incident Type-II Quantum Well Infrared Detector Using an Indirect AlAs/$Al_{0.5}Ga_{0.5}As$ System Grown on [110] GaAs,"Electronics Letts., 28(15) p.1468, July,16, 1992.

5. L. S. Yu, S. S. Li, Y. H. Wang, and Y. C. Kao,"A Study of Coupling Efficiency versus Grating Periodicity in A Normal Incident Grating-Coupled GaAs/AlGaAs Quantum Well Infrared Detector," J. Appl. Phys., 72(6), pp.2105, Sept. 15, 1992.

6. Y. H. Wang, S, S. Li, and P. Ho,"A Photovoltaic and Photoconductive Dual Mode Operation GaAs/AlGaAs Quantum Well Infrared Detector for Two Band Detection," Appl.Phys. Lett., 62(1), pp.93, Jan. 4 1993.

7. Y. H. Wang, S. S. Li, and P. Ho,"A Voltage-Tunable Dual Mode Operation InAlAs/InGaAs Bound-to-Miniband Transition QWIP for Narrow and Broad Band Detection at 10 μm," Appl. Phys. Lett., 62(6), pp.621 Feb. 8 , 1993.

8. P. Ho, P. A. Martin, L. S. Yu, and S. S. Li,"Growth of GaAs and AlGaAs on Misoriented (110) GaAs and a Normal Incidnece Type-II Quantum Well Infrared Detector," accepted, J. Vacuum Science and Technology, Oct., 1992.

9. S. S. Li, M. Y. Chuang and L. S. Yu,"Current Conduction Mechanisms in Bound-to-Miniband Transition III-V Quantum Well Infrared Photodetectors," ***Semiconductor Science and Technology***, vol.8, pp.406-411, 1993.

10. Y. H. Wang, Sheng S. Li, P. Ho, and M. O. Manasreh, "A Normal Incidence Type-II Quantum Well Infrared Photodetector Using An Indirect AlAs/AlGaAs System Grown on [110] GaAs for the Mid- and Long-Wavelength Multicolor Detection," J. Appl. Phys., July 15 issue, 1993.

11. Y. C. Wang and S. S. Li,"A Numerical Analysis of Double Periodic Reflection Metal Grating Coupler for Multiquantum Well Infrared Photodetectors," J. Appl.Phys., August 15, 1993.

12. Y. C. Wang and S. S. Li,"A Numerical Analysis of Double Periodic Reflection Metal Grating Coupler for Multiquantum Well Infrared Photodetectors," J. Appl.Phys., submitted July,1993.

13. Y. H. Wang, S. S. Li, J. Chu, and P. Ho, "An Ultra-low Dark Current Normal Incidence P-type Strained Layer InGaAs/InAlAs QWIP with Background Limited Performance (BLIP)," Appl. Phys. Lett., submitted, August, 1993.

2.3. Workshop and Conference Presentations

1. L. S. Yu, S. S. Li, and Pin Ho, " Largely Enhanced Intra-subband Absorption in a Wide InAlAS/InGaAs Quantum Well with a Short-Period Superlattice Barrier Structure,"paper presented at the ***SPIE's Symposium on Quantum Wells and Superlattices***, Somerset, NJ, 23-27 March,1992. Paper published in the SPIE Conference Proceeding.

2. S. S. Li and L. S. Yu, "Grating Coupled Bound-to-Miniband Transition III-V Quantum Well Infrared Detectors," **invited paper**, presented at ***the Innovative Long Wavelength Infrared Photodetector Workshop***, Jet Propulsion Lab., Pasadena, CA, April 7-9, 1992.

3. L. S. Yu and S. S. Li,"A Normal Incident Type-II Quantum Well Infrared Detector Using an Indirect AlAs/$Al_{0.5}Ga_{0.5}As$ System Grown on [110] GaAs, paper presented at ***the Innovative Long Wavelength Infrared Photodetector Workshop***, Jet Propulsion Lab., Pasadena, CA, April 7-9, 1992.

4. L. S. Yu, S. S. Li, Y. H. Wang, and P. Ho," Grating Coupled III-V Quantum Well Infrared Detectors Using Bound-to-Miniband Transition," paper presented at ***the SPIE Conference on Infrared Detectors and Focal Plane Arrays at OE/Aerospace Sensing 92***," Orlando, FL, April 20-24, 1992. Full paper published in the SPIE conference proceeding.

5. S. S. Li,"Grating Coupled Bound-to-Miniband Transition III-V Multiquantum Well Infrared Photodetectors," presented at the DARPA IR Detector Workshop, Washington D.C., June 12, 1992.

6. S. S. Li, M. Y. Chuang and L. S. Yu,"Current Conduction Mechanisms in Bound-to-Miniband Transition III-V Quantum Well Infrared Photodetectors," paper presented at the ***International Conference on Narrow Gap Semiconductors***, University of Southampton, Southampton, UK, July 19-23, 1992.

7. P. Ho, P. A. Martin, L. S. Yu, and S. S. Li,"Growth of GaAs and AlGaAs on Misoriented (110) GaAs and a Normal Incidnece Type-II Quantum Well Infrared Detector," paper presented at the ***12th North American Conference on Molecular Beam Epitaxy,*** Oct.12-14, 1992.

8. S. S. Li,"Novel Grating Coupled Miniband Transport III-V Multiquantum Well Infrared Photodetectors for Focal Plane Array Applications," presented at the DARPA IR Detector Workshop, Washington D.C., Dec 11, 1992.

9. S. S. Li, Y. H. Wang, M. Y. Chuang, P. Ho, , "Photoconductive and Photovoltaic Dual-Mode Operation III-V Quantum Well Infrared Photodetectors for 2 - 14 μm Detection," presented at the Materials Research Society (MRS), Symposium C2 on **Infrared Detectors**, San Francisco, April 12-16, 1993.

10. D. Wang, Y. H. Wang, G. Bosman and S. S. Li,"Noise Characterization of Novel Quantum Well Infrared Photodetectors," **Invited paper** to be presented at the ***12th Int. Conf. on Noise in Physical Systems and 1/f Fluctuations - The High Technologies Conference***, St. Louis, MO, August 16-20, 1993.

11. S. S. Li,"Some Novel High Performance III-V Quantum Well Infrared Photodetectors for Focal Plane Array Image Sensor Applications," **invited paper** to be presented at ***the NATO Advanced Research Workshop on Intersubband Transition Physics and Devices***, Whistler, Canada, September 7 - 10, 1993.

12. S. S. Li,"Grating Coupled III-V Quantum Well Infrared Photodetectors for Mid-Wavelength and Long-Wavelength Infrared Detection," **invited paper** to be presented at ***the First International Symposium on Long Wavelength Infrared Photodetectors*** in conjunction with the Fall Electrochemical Society (ECS) Meeting in New Orlean, LA, October 10 -15, 1993.

2.4 Interactions with Government and Industrial Laboratories

1. Continued to collaborate with Dr. Pin Ho of General Electric Co.,in Syracuse, NY, on the growth of III-V QWIP's structures by using the molecular beam epitaxy (MBE) technique.

2. Continued to collaborate and exchange technical information on QWIP results with Dr. Swami Swaminathan of A T & T Bell Lab., in Breinigsville, PA, on the planar metal grating coupler structure developed at the University of Florida for applications in the QWIP focal plane arrays.

3. Contiuned to interact and exchange technical information on QWIP results with Dr. M. Tidrow of U.S. Army Electronics Tech. & Devices Laboratory, EPSD, Fort Monmouth, NJ.

4. Dr. Li was invited to give a seminar at the Electronics Technology Laboratory, WPAFB, Ohio, on ***The bound-to-miniband transition III-V QWIPs*** on August 21, 92, and discussed with Dr.Omar Manasreh and his colleagues in the Electronics Technology Laboratory at the WPAFB. Dr. Manasreh had performed optical absorption measurements on Dr. Li's QWIP samples, while Dr. Li has fabricated and characterized some QWIP samples provided by Dr. Manasreh. Dr. Li is currently writing a book chapter on grating coupled miniband transport QWIPs for a new book on ***Long Wavelength Quantum Well Infrared Photodetectors*** edited by Dr. Manasreh and to be published by Artech Publishing Co.

5. Dr. Li was invited by the American Engineering Education Association (AEEA) to serve on a review panel for Naval Postdoctoral Fellowship program in Washington D.C., August 7, 92, to review a dozen of proposals submitted by various applicants.

6. Mr. Tom Briere of InfraMetrics has contacted Dr. Li, expressing his interest in using our QWIPs in the infrared imaging sensor applications. Dr. Li has sent a copy of his most recent ARPA quarterly progress report to Mr. Briere. Dr. Li will keep in touch with InfraMetrics on our new development in QWIP arrays.

III. Technical Results

3.1 An Ultra-low Dark Current P-type Strained-layer InGaAs/InAlAs Quantum Well Infrared Photodetector With Background Limited Performance (BLIP)

Summary: An ultra-low dark current normal incidence p- strained-layer $In_{0.3}Ga_{0.7}As/In_{0.52}Al_{0.48}As$ quantum well infrared photodetector (PSL-QWIP) grown on semi-insulating (100) InP by MBE for 8-12 μm detection has been developed. This PSL-QWIP shows background limited performance (BLIP) for $T \leq 90$ K, which is the highest BLIP temperature ever reported for the QWIPs. Due to the lattice mismatch between the substrate and the quantum well a biaxial tensile strain is introduced in the quantum well layers, and the inversion of the light- and heavy-hole bands occurs. As a result, the light-hole state becomes the ground state for free holes with small effective mass, thereby greatly enhance the valence intersubband absorption. The BLIP detectivity D^*_{BLIP} for this PSL-QWIP was found to be 5.9×10^{10} $cm \cdot \sqrt{Hz}/W$ at $\lambda_p = 8.1$ μm, $V_b = -2V$, and T = 77 K.

3.1.1 Introduction

Quantum well infrared photodetectors using n-type GaAs/AlGaAs and InGaAs/InAlAs systems for 8-14 μm have been extensively studied in recent years[1-2]. With low electron effective mass and high electron mobility, the n-type GaAs and InGaAs QWIPs offer excellent IR detection properties. However, the quantum mechanical selection rule for the intersubband transition requires that the radiation electric field has a component perpendicular to the quantum well plane (i.e., z-direction) in order to induce intersubband absorption in the quantum wells. As a result, for focal plane array (FPA) applications, the use of planar metal or dielectric grating structures for coupling IR radiation into the quantum well[2-4] becomes necessary to allow normal incidence illumination for the n-type QWIPs.

P-type QWIPs using valence intersubband transitions have been demonstrated recently in the lattice-matched GaAs/AlGaAs and InGaAs/InAlAs material systems[5-7]. Due to a mixing between the light hole states and heavy hole states, the normal incident illumination is allowed for the intersuband transition in p-type QWIPs. In general, intersubband transitions under normal incident radiation in p-type quantum well are induced by linear combination of p-like valence-band Bloch states which provides a nonzero coupling between this component and normal radiation field. The strong mixing between light and heavy hole states greatly enhances the normal incidence intersubband absorption. However, in the lattice-matched quantum well systems, this intersubband

transition occurs between the heavy hole ground state and the upper excited states. Due to the relatively large heavy hole effective mass, relative weak absorption and low responsivity are expected in the IR wavelength range. If a tensile strain is introduced between the quantum well and the barrier layers[13-14], the effect of tensile strain can cause heavy-hole state and light-hole ground state inverted. This in turn will cause the intersubband transition from the populated light-hole ground state to the upper energy band states. Since the light hole has a small effective mass (comparable to the electron effective mass), the optical absorption and the responsivity of p-type QWIPs can be greatly enhanced by using this approach.

3.1.2 Theory

If we intentionally introduce biaxial stresses between the well layers and the barrier layers in a p-type strained layer QWIP structure, the pseudomorphic or coherent heterointerfaces can be grown if the layer thickness is within the critical thickness. The strained-layers have the same in-plane lattice constant $a_{||}$ (i.e., $a_{x,y}$), and store the excess energy equal to the elastic strain energy within the layers. The in-plane lattice constant $a_{||}$ can be expressed by[8]

$$a_{||} = a_1 \left[1 + \delta_o / \left(1 + \frac{\xi_1 L_1}{\xi_2 L_2} \right) \right], \tag{1}$$

where $a_{1,2}$ and $L_{1,2}$ are the individual layer lattice constant and thickness, respectively. ξ is the shear moduli given by $\xi = (C_{11} + C_{12} - 2C_{12}^2/C_{11})$, where C_{ij} are the elastic constants which can be found in reference[9]. δ_o is the lattice mismatch between the layers defined by $\delta_o = (a_2 - a_1)/a_1$ (assuming $a_2 > a_1$). If the QWIP structure is grown along [100] direction and the strained-layer is within critical layer thickness L_c, the components of the strain tensor [e] are reduced to

$$e_{xx} = e_{yy} = e_{||}; e_{zz} = -e_{||} \left(\frac{2C_{12}}{C_{11}} \right), \tag{2}$$

$$e_{xy} = e_{yz} = e_{zx} = 0. \tag{3}$$

The strain induced energy band shifts for conduction, heavy-hole, and light-hole bands, respectively, can be approximated by

$$\Delta E_c = 2V_c \frac{C_{11} - C_{12}}{C_{11}} \delta_o \tag{4}$$

$$\Delta E_{lh} = V_s \frac{C_{11} + 2C_{12}}{C_{11}} \delta_o \tag{5}$$

$$\Delta E_{hh} = -\Delta E_{lh} \tag{6}$$

where V_c and V_s are the conduction band deformation potential and shear deformation potential[9]. The total hydrostatic deformation potential V (= V_c + V_v, V_v for valence band deformation

potential) can be expressed by[10]

$$V = V_c + V_v = -\frac{1}{3}(C_{11} + 2C_{12})\frac{dE_g^o}{dP} \tag{7}$$

where dE_g^o/dP is the unstrained energy bandgap change with respect to the unit pressure. The strain considerably affects the energy band structure and induces the splitting between the heavy-hole band and the light-hole bands in the valence band zone-center[11] (i.e., in-plane wavevector $k_{||}$ = 0), which is degenerated in the unstrained case. When tensile strain is applied between the quantum well and the barrier layer[12-14] along the superlattice growth direction, the tensile strain can push the light-hole state upward and pull the heavy-hole state downward. As a result, heavy-hole states and light-hole states can be inverted under a certain strain and quantum well thickness. This in turn will cause the intersubband transition from the populated light-hole ground state to the upper energy band states. Since the light hole has a small effective mass (comparable to the electron effective mass), the optical absorption and photon responsivity in the p-type QWIPs can be greatly enhanced by using this new approach.

3.1.3 Results and Discussion

In this section we disucss a new normal incidence p-type strained layer (PSL) $In_{0.3}Ga_{0.7}As/In_{0.52}Al_{0.48}As$ QWIP using th. ground light-hole state to the heavy-hole state intersuband transition. Figure 3.1.1 shows the energy band diagram for the PSL-QWIP, which illustrates the energy bending due to the dopant migration effect during the layer growth. The PSL-QWIP structure was grown on a (100) semi-insulating (SI) InP substrate using MBE technique. Beryllium was used as the p-type dopant and the structure consists of 20 periods of 4-nm $In_{0.3}Ga_{0.7}As$ quantum well with a dopant density of 1×10^{18} cm^{-3} separated by 45-nm $In_{0.52}Al_{0.48}As$ undoped barrier layer. A 0.3 μm cap layer and a 1μm buffer layer of $In_{0.53}Ga_{0.47}As$ were grown with a dopant density of 2×10^{18} cm^{-3} for ohmic contacts. The contact and barrier layers are lattice-matched with the SI InP substrate, and the quantum well layer is in biaxial tension with a lattice mismatch of approximately 1.5% between the well and the barrier. In order to measure the spectral responsivity and dark current of the PSL-QWIP, a 200 by 200 μm^2 mesa structure was created by using the chemical etching process. Au/Zn alloy was used to make ohmic contacts on p-type InGaAs/InAlAs QWIP. The ohmic contacts were thermally evaporated onto the QWIP mesas with a thickness of 0.12 μm. The QWIPs were then annealed at 480 °C for two minutes to obtain stable and low contact resistance.

Figure 3.1.2 shows the measured 77 K dark current density and 300 K background photocurrent

density for the PSL-QWIP. Asymmetric dark current characteristic for the PSL-QWIP was observed due to the energy band bending effect as shown in Fig.3.1.1. Due to the extremely low dark current, this PSL-QWIP is under background limited performance (BLIP) for the field of view (FOV) 90° at T $\leq$ 90 K with applied bias between -2.5 V and +5 V or higher, which was **the highest BLIP temperature ever reported for the QWIPs**. The responsivity of the QWIP was measured as a function of temperature, bias voltage, and wavelength using a globar and automatic PC-controlled single-grating monochrometer system under normal incidence IR illumination. The measured photocurrent versus radiation wavelength for both positive and negative biases are shown in Fig. 3.1.3(a) and (b), respectively. A peak response wavelength at $\lambda_p = 8.1$ μm was observed in the long-wavelength infrared (LWIR) detection band, which is attributed to the intersubband transition between the confined ground light-hole state to the continuum heavy-hole band states. The cutoff wavelength for this QWIP was found to be $\lambda_c = 8.8$ μm with a spectral bandwidth of $\Delta\lambda/\lambda_p = 12\%$. Since the two heavy-hole sub-bands are confined in the wells with very low tunneling probability off the thicker barrier layer, the photoresponse from these heavy-hole states was not detected.

In a BLIP limited QWIP, the dominant noise source is the photon noise while all other noise sources are negligible in comparison. The photon noise is calculated based on the arrival statistics of the incoherent photons. The background photon noise current i_{np} is given by[15,16]

$$i_{np}^2 = 4e^2\eta g^2(P_b/2)B/(h\nu), \tag{8}$$

where P_b is the incident background optical power, B is the QWIP bandwidth, η is the absorption quantum efficiency, ν is the incident photon frequency, and g is the photoconductive gain. The optical photosignal current I_p can be approximated by

$$I_p = (e/h\nu)\eta g(P_s/2), \tag{9}$$

where P_s is the incident optical signal power. The factor of 1/2 inside the parenthesis of P_b and P_s given in the above two equations is due to the incident optical polarization selectivity for n-type QWIPs (without 1/2 for p-type QWIPs). By setting the signal-to-noise power ratio equal to unity, the background-limited noise equivalent power $(NEP)_{BLIP}$ and detectivity D^*_{BLIP} for n-type QWIPs can be expressed by

$$(NEP)_{BLIP} = 2\sqrt{2h\nu BP_b/\eta}, \tag{10}$$

$$D^*_{BLIP} = \sqrt{AB}/(NEP)_{BLIP} = (1/2)\frac{\lambda_p}{\sqrt{2}hc}\left(\frac{\eta}{Q_b}\right)^{1/2}, \tag{11}$$

where A is the active area of the detector, and $Q_b = P_b/(A\ h\nu)$ is the incident photon flux from the background for a given spectral bandwidth $\Delta\nu$ and a peak wavelength λ_p. Q_b is given by

$$Q_b = \frac{2\pi}{c^2}\frac{\nu^2\Delta\nu}{e^{h\nu/KT}-1}sin^2\left(\frac{\theta}{2}\right), \tag{12}$$

where θ is the field of view (FOV). For p-type QWIPs, a factor of $\sqrt{2}$ is used in the above detectivity expression D^*_{BLIP} since p-type QWIPs can absorb both optical polarizations of the IR radiation.

For a non-BLIP QWIP, since the electronic noise from the detector is no longer negligible, the term Q_b should be replaced by $(Q_b + Q_d)$, where Q_d is the equivalent photon flux which generates the same level of the electronic noise. Thus, the detectivity can be calculated by

$$D^* = \frac{\lambda_p}{2hc}\frac{\eta\sqrt{g}}{\sqrt{J_d/e}} \tag{13}$$

where J_d is the dark current density. It is noted that the detectivity D^* for a non-BLIP detector depends photoconductive gain g while the detectivity for the BLIP is independent of g.

The responsivity for the PSL-QWIP was calibrated by using a standard pyroelectric detector and lock-in amplifier technique. Asymmetric responsivities of 34 mA/W at bias + 4 V and 51 mA/W at bias - 4 V were obtained. The maximum BLIP detectivity D^*_{BLIP} at $\lambda_p = 8.1\ \mu m$ was calculated to be 5.9×10^{10} cm $Hz^{1/2}/W$ with a responsivity $R_A = 18$ mA/W at bias + 2 V, FOV = 90° and T = 77 K. The quantum efficiency for the PSL-QWIP was estimated from the responsivity measurement and a reasonable photoconductive gain g = 0.015 was used in the BLIP detectivity calculation. When the Johnson noise and the readout noise are ignored, the %BLIP for positive and negative bias are evaluated by using

$$\%BLIP \approx \frac{i_{np}}{(i^2_{np}+i^2_{nd})^{1/2}} \tag{14}$$

where $i_{np,nd}$ are the 300 K background photocurrent noise and dark current noise, respectively. Figure 3.1.4 shows the calculated %BLIP for the positive and negative biases. A nearly full BLIP detection was achieved at bias voltages less than |2| V. As a result of the fully BLIP detection in our PSI-QWIP, the noise equivalent temperature difference (NEΔT) is expected to improved significantly for the focal plane array thermal imaging applications.

In conclusion, we have demonstrated a new ultra-low dark current normal incidence p-type strained layer InGaAs/InAlAs QWIP with BLIP detection for $T \leq 90K$. The BLIP detectivity of our PSL-QWIP was greatly enhanced due to the biaxial tensile strain introduced in this QWIP

structure. By further optimizing the quantum well dopant density, biaxial strain strength, and structure parameters, the PSL-QWIPs can be used for 8-14 μm long-wavelength large size focal plane array image sensor system with BLIP detection at $T \geq 77K$.

References

1. B. F. Levine, R. J. Malik, J. Walker, K. K. Choi, C. G. Bethea, D. A. Kleinman, and J. M. Vandenberg, Appl. Phys. Lett. **50**, 273 (1987).
2. L. S. Yu, S. S. Li, Appl. Phys. Lett. **59**, 1332 (1991).
3. G. Hasnain, B. F. Levine, C. G. Bethea, R. A. Logan, J. Walker, and R. J. Malik, Appl. Phys. Lett. **54**, 2515 (1989).
4. J. Y. Andersson and L. Lundqvist, J. Appl. Phys. **71**, 3600 (1992).
5. B. F. Levine, S. D. Gunapala, J. M. Kuo, S. S. Pei, and S. Hui, Appl. Phys. Lett. **59**, 1864 (1991).
6. J. Katz, Y. Zhang, and W. I. Wang, Electron. Lett. **28**, 932 (1992).
7. W. S. Hobson, A. Zussman, B. F. Levine, and J. deJong, J. Appl. Phys. **71**, 3642 (1992).
8. J. W. Matthews and A. E. Blakeslee, J. Cryst. Growth **32**, 265 (1976).
9. Landlt-Börnstein, Numerical Data and Functional Relationships in Science and Technology, O. Madelung, ed. Group III, **17**, Springer-Verlag, Berlin (1982).
10. G. Ji, D. Huang, U. K. Reddy, T. S. Henderson, R. Houre, and H. Morkoç, J. Appl. Phys. **62**, 3366 (1987).
11. T. P. Pearsall, Semiconductors and Semimetals, **32**, 55 (1990).
12. H. Asai, and Y. Kawamura, Appl. Phys. Lett. **56**, 746 (1990).
13. H. Xie, J. Katz, and W. I. Wang, Appl. Phys. Lett. **59**, 3601 (1991).
14. R. T. Kuroda and E. Garmire, Infrared Phys. **34**, 153 (1993).
15. B. F. Levine, C. G. Bethea, G. Hasnain, J. Walker, and R. J. Malik, Appl. Phys. Lett., **53**, 296 (1988).
16. D. A. Scribner, M. R. Kruer, and J. M. Killiany, Proc. of the IEEE, **79**, 66 (1991).

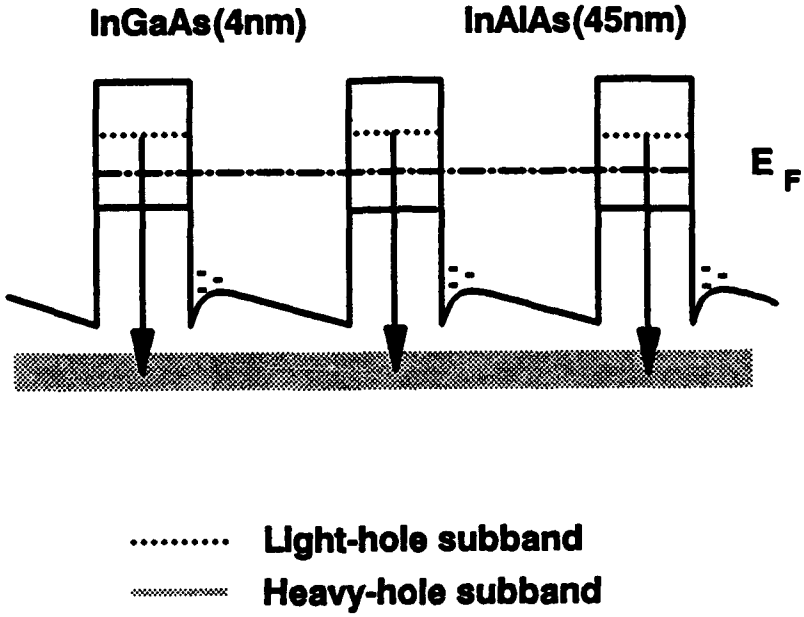

Figure 3.1.1. The schematic energy band diagram for the p-type strained layer (PSL) InGaAs/InAlAs QWIP taking into consideration of band bending effect due to doping migration (valence band offset equals 140 meV).

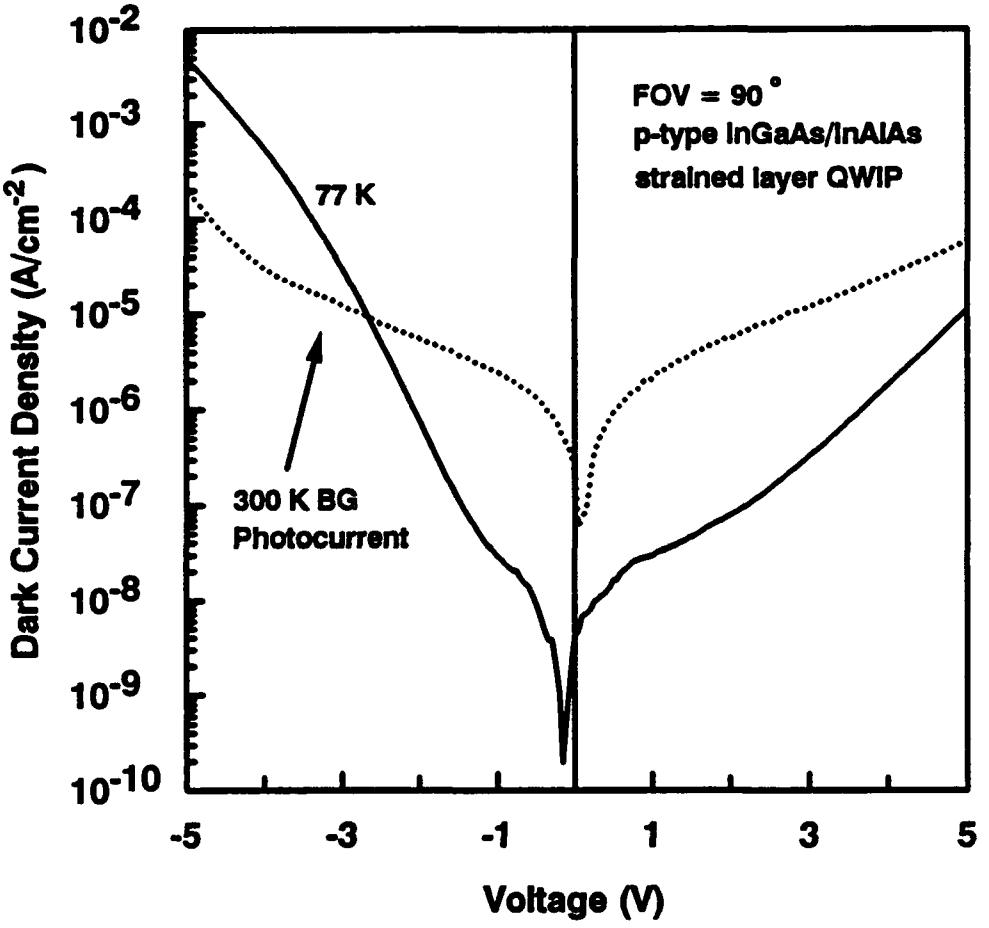

Figure 3.1.2 Measured 77 K dark current density and 300 K background photocurrent density for the PSL-QWIP at FOV = 90 °.

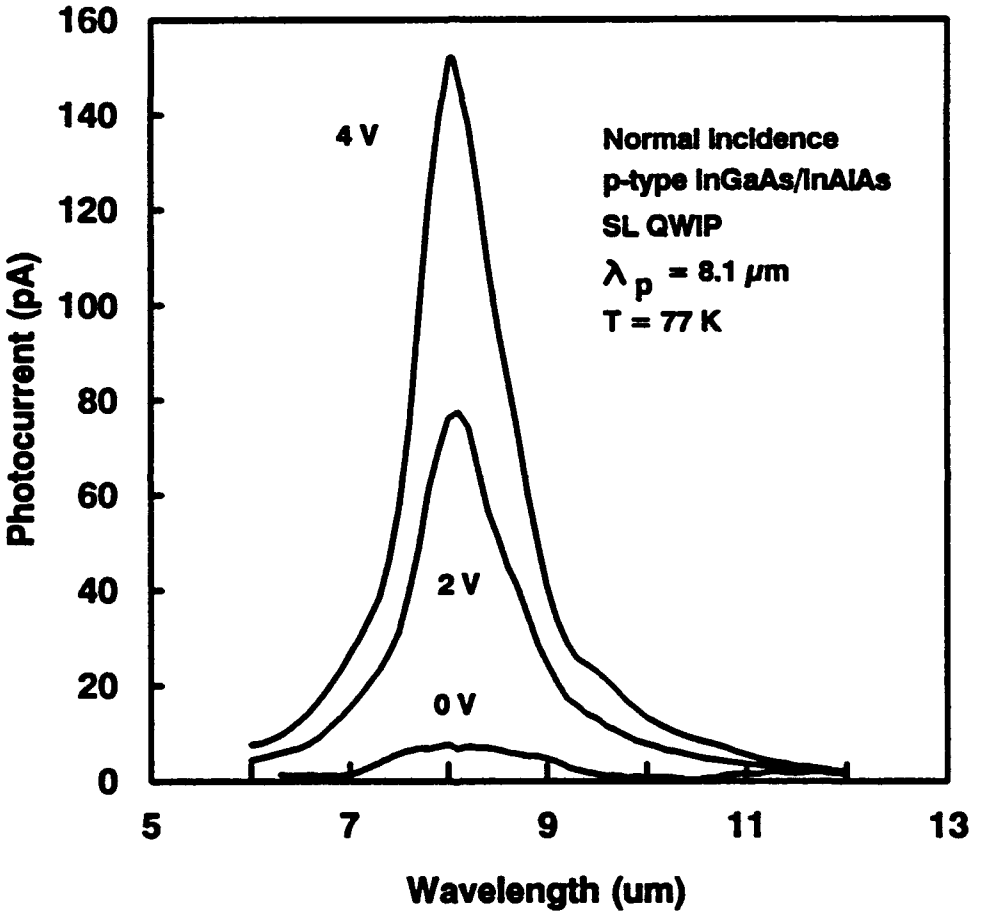

Figure 3.1.3a The measured photocurrent versus wavelength under different positive biases for the PSL-QWIP.

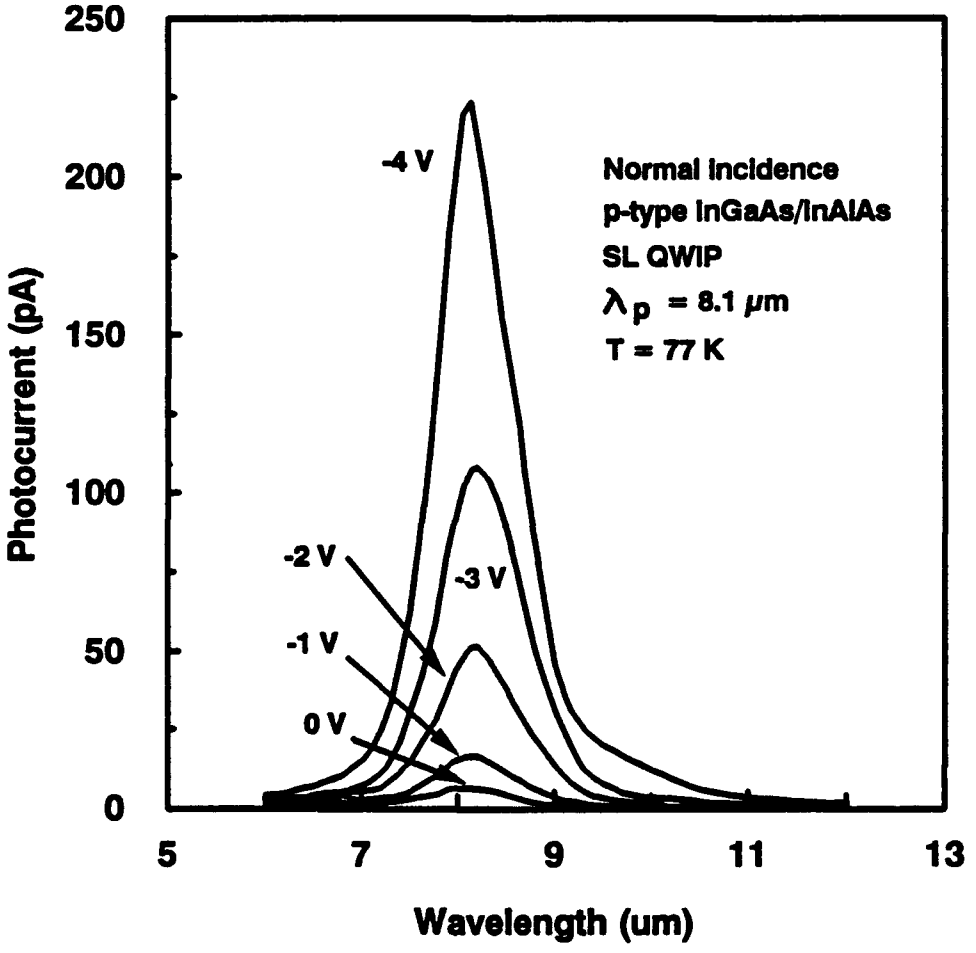

Figure 3.1.3b The measured photocurrent versus wavelength under different negative biases for the PSL-QWIP.

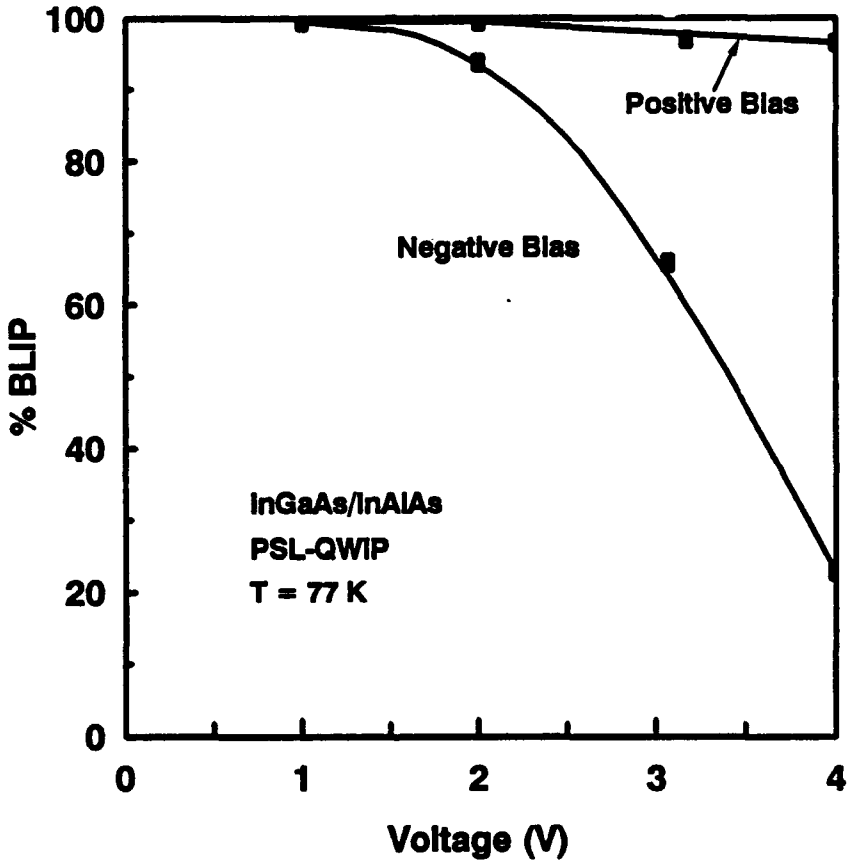

Figure 3.1.4. % BLIP of the PSL-QWIP versus applied bias voltage for the positive and negative bias cases, measured at T = 77 K.

3.2 Background Limited Performance (BLIP) for the QWIPs

3.2.I Introduction

Recently, focal plane arrays (FPAs) using GaAs quantum well infrared photodetectors (QWIPs) for thermal imaging have been demonstrated[1,2]. However, the operating temperature of these QWIP FPAs has to keep at 60 K due to the large dark current observed in these QWIPs at 77 K. In order to realize the background limited photocurrent (BLIP) performance at T = 77 K, it is required to reduce the dark current of the QWIP by several orders of magnitude while maintaining its high detectivity.

3.2.2 BLIP Detectivity

Under BLIP condition, the dominant noise source is the photon noise while all other noise sources are negligible in comparison. The photon noise is calculated based on the arrival statistics of the incoherent photons. The background photon noise current i_p can be expressed as[3,4]

$$i_{np}^2 = 4e^2\eta g^2(P_b/2)B/(h\nu), \tag{15}$$

where P_b is the incident background optical power, B is the QWIP bandwidth, η is the absorption quantum efficiency, ν is the incident photon frequency, and g is the photoconductive gain. The photosignal current I_p can be approximated by

$$I_p = (e/h\nu)\eta g(P_s/2), \tag{16}$$

where P_s is the incident optical signal power. A factor of 1/2 is included in the P_b and P_s term of the above two equations, which takes into account the incident optical polarization selectivity for n-type QWIPs (without 1/2 for the p-type QWIPs). By setting the signal-to-noise power ratio equal to unity, we can determine the background-limited noise equivalent power $(NEP)_{BLIP}$ and the detectivity D^*_{BLIP} for the n-type QWIPs, which are given by

$$(NEP)_{BLIP} = 2\sqrt{2h\nu BP_b/\eta}, \tag{17}$$

$$D^*_{BLIP} = \sqrt{AB}/(NEP)_{BLIP} = (1/2)\frac{\lambda_p}{\sqrt{2}hc}\left(\frac{\eta}{Q_b}\right)^{1/2}, \tag{18}$$

where A is the active area of the detector, and $Q_b = P_b/(Ah\nu)$ is the incident photon flux from the background radiation for a given spectral bandwidth $\Delta\nu$ and a peak wavelength λ_p. Q_b is given by

$$Q_b = \frac{2\pi}{c^2}\frac{\nu^2\Delta\nu}{e^{h\nu/KT}-1}\sin^2\left(\frac{\theta}{2}\right), \tag{19}$$

where θ is the field of view (FOV). For p-type QWIPs, a factor of $\sqrt{2}$ is needed in the detectivity expression D^*_{BLIP} since p-type QWIPs can absorb both optical polarizations of the incident IR radiation.

For a non-BLIP QWIP, since electronic noise from the detector is no longer negligible, the Q_b term should be replaced by $(Q_b + Q_d)$, where Q_d is the equivalent photon flux which can generate the same level of the electronic noise. Thus, the detectivity can be calculated by using the expression given by

$$D^* = \frac{\lambda_p}{2hc}\frac{\eta\sqrt{g}}{\sqrt{J_d/e}} \tag{20}$$

where J_d is the dark current density. It is noted that the detectivity D* for a non-BLIP QWIP depends on photoconductive gain, g, whereas the detectivity for the BLIP is independent of g.

In an ideal broadband PC mode detector such as the conventional interband detectors, the detectivity D^*_{BLIP} is only slightly higher than that of a narrow band PC mode QWIP under same operation conditions. Thus, the polarization loss for half of the IR incident power in n-type QWIPs is partially compensated by the narrow bandwidth of the QWIPs, while p-type QWIPs will produce higher BLIP detectivity due to their very narrow spectral bandwidth and without losing the polarization of the incident power. The BLIP noise performance for a PV mode detector compared to a PC mode detector is a factor of $\sqrt{2}$ better because the PC mode detector has the generation and recombination fluctuation noise, while the PV mode detector sweeps the photoexcited carriers out of the detector before recombination takes place.

3.2.3 BLIP Measurements

In QWIP thermal imaging focal plane arrays, the total current in the readout electronic circuits consists of both the dark current and 300 K background photocurrent. Under BLIP conditions, the dark current of the QWIP at 77 K should be much smaller than the 300 K background photocurrent in order to obtain high quality thermal imaging at 77 K operation.

To measure the dark current of the QWIPs without the background photocurrent contribution, the detectors can be placed in a low-temperature environment such as at 77 K by using cold-shielding technique[5] or by immersing the QWIPs in liquid nitrogen. On the other hand, the 300 K background photocurrent measurement was performed by placing the detector in a cryogenic system with a certain angle of field of view, and the maximum BLIP temperature can be found when the detector photocurrent remains constant as the detector's temperature is decreased.

Figure 3.2.1 shows the measured dark current and 300 K background photocurrent for five different QWIPs developed in our Lab: (a) p-type strained layer (PSL)InGaAs/InAlAs QWIP, (b) GaAs/AlGaAs dual mode (DM) operation QWIP, (c) type-II AlAs/AlGaAs QWIP, (d) voltage tunable dual-mode (VTDM) operation InGaAs/InAlAs QWIP, and (e) step-bound-to-miniband (SBTM) InGaAs/AlGaAs/GaAs QWIP. The SBTM, VTBM, and type-II QWIPs reach the BLIP condition for T $\leq$ 60 K, while the PSL- and DM-QWIPs are BLIP limited at T $\leq$ 90 K and 77 K, respectively, which are by far the highest BLIP temperature obtained for the QWIPs. Table. I summarizes the structure parameters, responsivities, detectivities, and BLIP temperatures for the five III-V QWIPs developed in our Lab.

3.2.4 Results and Discussion

The performance of the GaAs DM-QWIP has been reported by us earlier[6]. In the GaAs DM-QWIP, a very low dark current density was obtained at low bias voltage (see Fig 3.2.2a) due to the use of enlarged AlGaAs barrier layer between the quantum wells, and the BLIP detection at T = 77 K was achieved at a bias between -1.2 V and +0.7 V ("-" means the top mesa is negatively biased). The PC mode BLIP detectivity D^*_{BLIP} for λ_p = 12 μm was found to be about 2×10^{10} cm $Hz^{1/2}/W$ at bias 1 V, which is slightly lower than that (3.1×10^{10} cm $Hz^{1/2}/W$) for an ideal PC mode broadband detector under η = 0.5 and field of view $\theta = 180^o$ at the same peak wavelength. However, the PV mode BLIP detectivity at λ_p = 7.7 μm is much smaller than the value of an ideal PV mode broadband detector due to low internal built-up field.

The performance characteristics of a normal incidence p-type strained-layer (PSL) InGaAs QWIP has been described in Section 3.1. In a p-type strained-layer $In_{0.3}Ga_{0.7}As/In_{0.52}Al_{0.48}As$ QWIP grown on InP substrate, the intervalence subband ground state was inverted from the heavy-hole state to light-hole state by using biaxial tensile strain in the quantum wells. The intervalence subband absorption was significantly enhanced (by about a factor of 3) due to the small effective mass and large mobility of the light holes. The excited light holes transport in 3-D heavy hole miniband above the barrier. The extremely low dark current density for the PSL-QWIP as shown in Fig. 3.2.2 (b) was obtained, which is mainly resulted from the very narrow heavy hole miniband conduction. A PC mode absorption peak at λ_p = 8.1 μm was observed, which showed the BLIP limited detection for T $\leq$ 90 K and bias between -2.6 V and +5 V. This 90 K BLIP temperature is by far the highest value ever achieved in a QWIP. The BLIP detectivity at λ_p = 8.1 μm was found to be 5.9×10^{10} cm $Hz^{1/2}/W$ for η = 1/2 and FOV = 90° at V_b = 2 V and T = 90 K, which

is the ideal PC mode broadband BLIP detectivity value for $\eta = 1/2$ and FOV = 180°. When the Johnson noise and the readout noise are ignored, % BLIP for the positive and negative bias are evaluated by using

$$\%BLIP \approx \frac{i_{np}}{(i_{np}^2 + i_{nd}^2)^{1/2}} \tag{21}$$

where $i_{np,nd}$ are the 300 K background photocurrent noise and dark current noise, respectively. The calculated %BLIP for the positive and negative bias for the PSL-QWIP is shown in Figure 3.1.4. A near 100 % BLIP detection was obtained at bias voltages less than |2| V. As a result of the fully BLIP detection for this PSL-QWIP, the noise equivalent temperature difference (NEΔT) will be significantly improved in the thermal imaging PSL-QWIP arrays. By using the PSL-QWIP described in Section 3.1, a normal incidence, high performance, and large-area focal plane array (FPA) operating at 77 K and under BLIP condition can be achieved for 8-12 μm applications.

References

1. C. G. Bethea, B. F. Levine, V. O. Shen, R. R. Abbott, and S. J. Hseih, IEEE, Trans., **ED-38**, 1118 (1991).
2. L. J. Kozlowski, G. M. Williams, G. J. Sullivan, C. J. Sullivan, C. W. Farley, R. J. Anderson, J. Chen, D. T. Cheung, W. E. Tannant, R. E. DeWames, IEEE, Trans., **ED-38**, 1124 (1991).
3. B. F. Levine, C. G. Bethea, G. Hasnain, J. Walker, and R. J. Malik, Appl. Phys. Lett., **53**, 296 (1988).
4. D. A. Scribner, M. R. Kruer, and J. M. Killiany, Proc. of the IEEE, **79**, 66 (1991).
5. V. Gopal and K. C. Chhabra, Infrared Phys., **31**, 333 (1991).
6. Y. H. Wang, S. S. Li, and Pin Ho, Appl. Phys. Lett., **62**, 93 (1993).

Table 3.2.1 Summary of the peak and cutoff wavelengths, responsivities,detectivities, and BLIP temperatures for five different QWIPs developed in our Lab.

QWIP	λ_p (μm)	R (A/W)	λ_c (μm)	D* cm-Hz$^{1/2}$/W	BLIP
DM	12 (PC)	0.48	13.2	†2.0×10^{10}	77K
	7.7 (PV)	11,000 (V/W)	8.5	†1.5×10^{9}	
VTDM	10.3 (PC)	0.038	11.7	5.8×10^{9}	45K
	10 (PV)	12,000 (V/W)	10.4	5.7×10^{9}	
SBTM	10 (PC)	0.11	11.3	4.3×10^{9}	55K
Type-II	2.2 (PC)	110	2.45	1.1×10^{12}	50K
	2.2 (PV)	64,000 (V/W)	2.45	1.4×10^{10}	
	3.5 (PC)	18.3	4.3	3.0×10^{11}	
	3.5 (PV)	58,000 (V/W)	4.3	1.2×10^{10}	
	12.5 (PC)	0.024	14.8	1.1×10^{9}	
PSL	8.1 (PC)	0.018	8.8	†5.9×10^{10}	90K

†: These values are for the background limited performance D^*_{BLIP}.

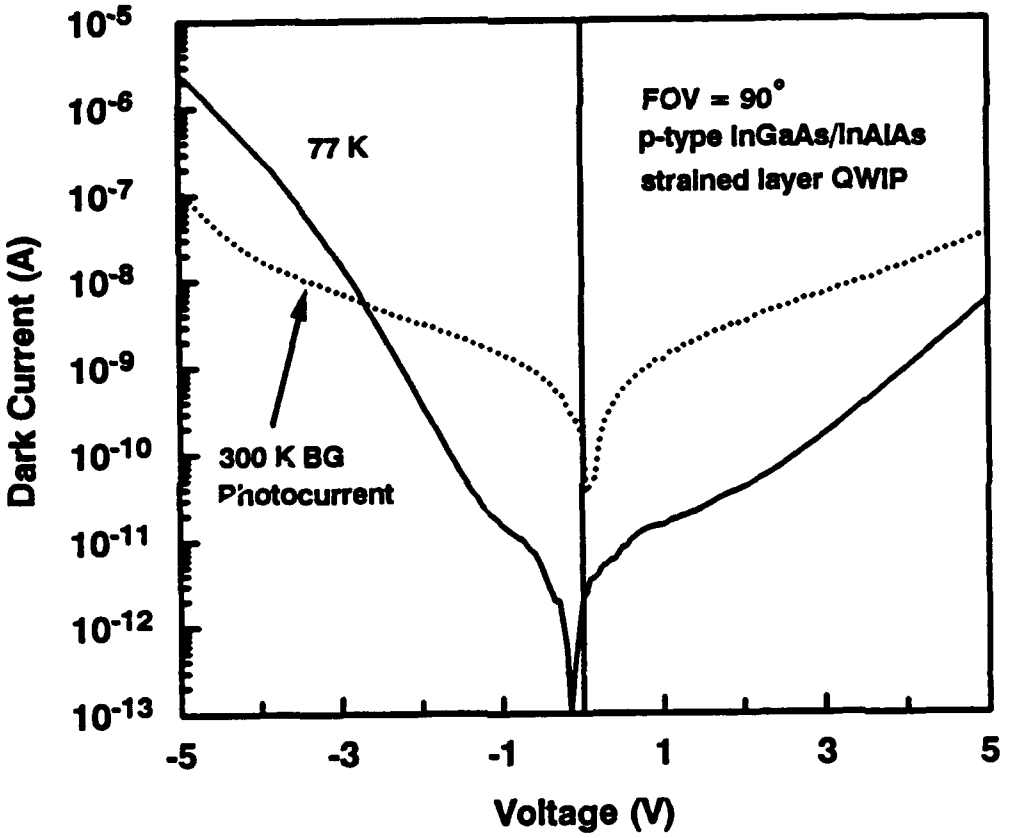

Figure 3.2.1a The measured 77 K dark current and 300 K background photocurrent versus bias voltage for a p-type strained layer InGaAs/InAlAs QWIP.

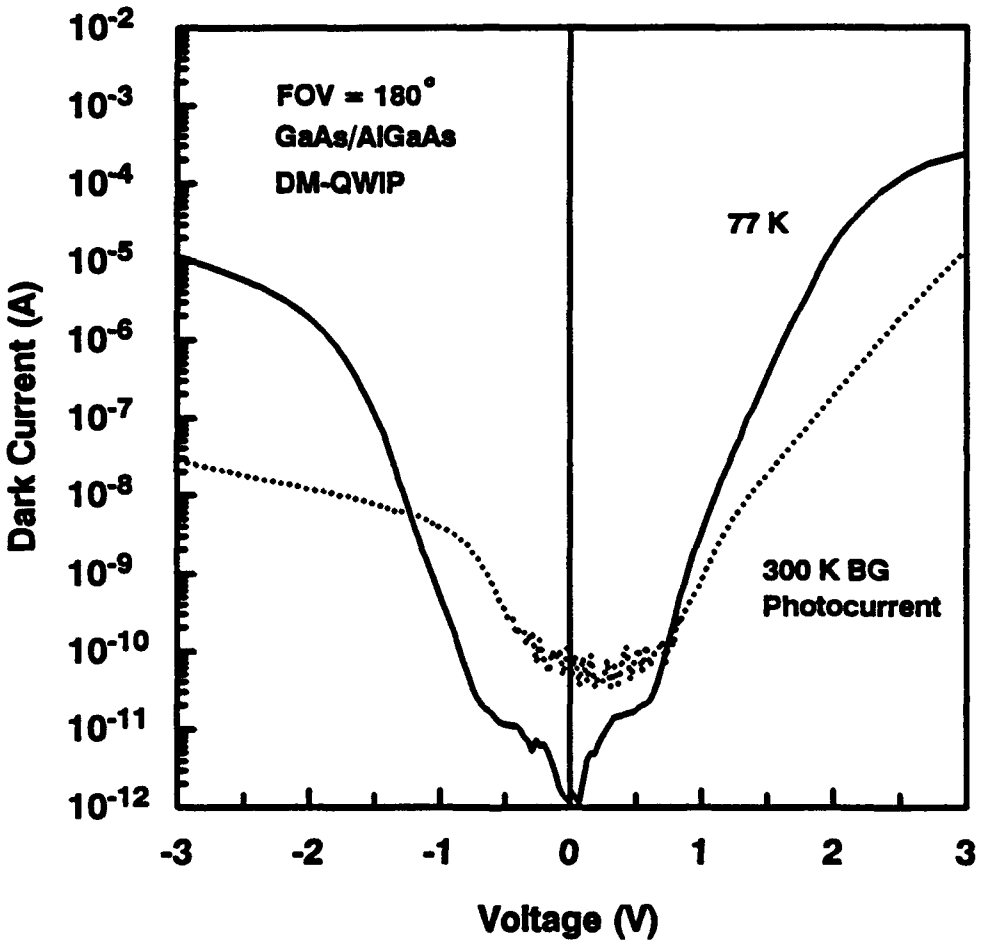

Figure 3.2.1b The measured 77 K dark current and 300 K background photocurrent versus bias voltage for a GaAs/AlGaAs DM-QWIP.

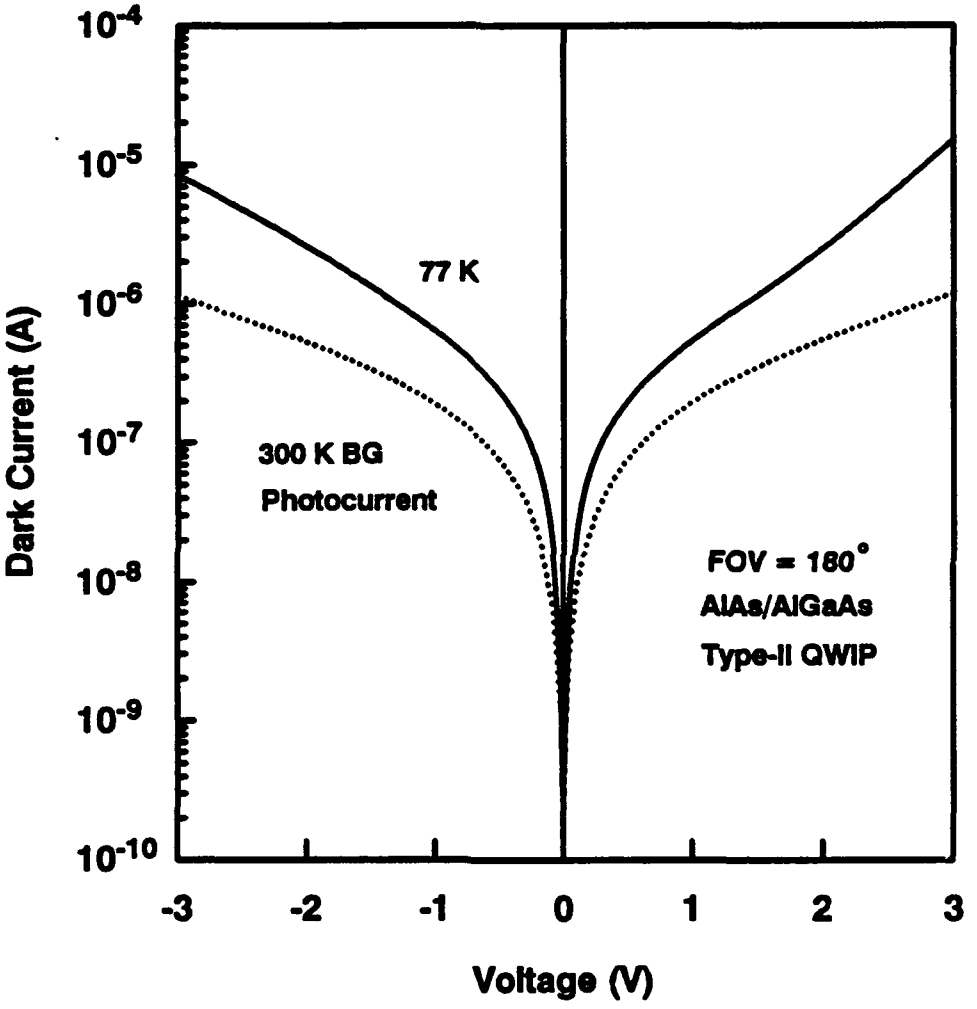

Figure 3.2.1c The measured 77 K dark current and 300 K background photocurrent versus bias voltage for a type-II AlAs/AlGaAs QWIP.

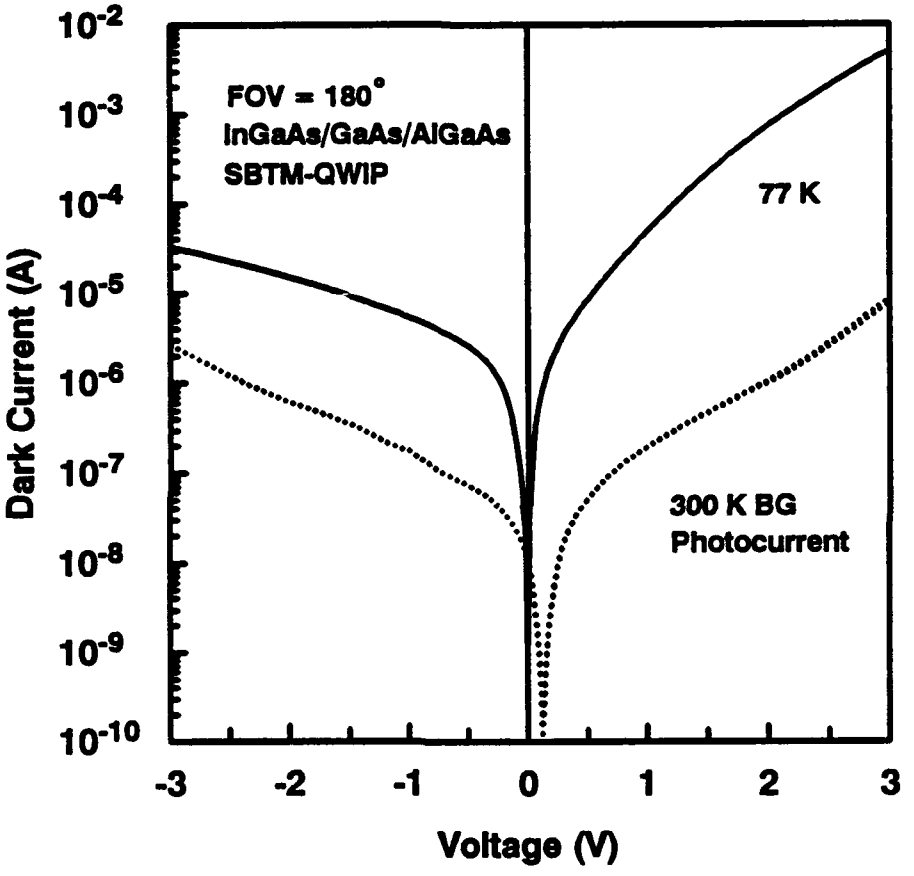

Figure 3.2.1d The measured 77 K dark current and 300 K background photo-current versus bias voltage for an InGaAs SBTM- QWIP.

3.3 Enhancement of Responsivity in an InGaAs Step-Bound-To-Miniband (SBTM) QWIP Using a 2-D Square Mesh Metal Grating Coupler

Summary: A theoretical and experimental study of the responsivity and coupling quantum efficiency in an InGaAs SBTM QWIP by using a planar 2D square mesh metal grating coupler has been carried out. The measured responsivity under back side illumination is 1.65 times higher than that under front side illumination. A maximum responsivity of $R_I = 0.5A/W$ was obtained using a grating period, $g = 3.3\mu$m and aperture width, $a = 2\mu$m at $\lambda = 10.4\mu$m under back side illumination.

3.3.1 Introduction

The main obstacle encountered in a type-I QWIP is that the electric field vector of the incident infrared (IR) radiation must have a component perpendicular to the quantum well layer planes to satisfy the selection rules of quantum mechanical intersubband infrared absorption. To enhance the absorption of normal incident IR light, a new grating coupler structure using 2D double period square metal mesh has recently been proposed. It is shown theoretically that a high grating coupling efficiency up to 70% is possible provided that the normalized aperture width a/g is equal to 0.6 and the grating period is properly chosen. In this section, we report the results of our theoretical and experimental study of such a 2D grating coupler applied to the InGaAs SBTM QWIP.

A schematic diagram of the 2D square mesh metal grating coupler is shown in Fig.3.3.1. When a plane wave IR radiation strikes on the grating under normal incident illumination, the IR radiation is scattered into several higher order diffracted waves whose wave vectors have parallel components equal to integer multiples of the reciprocal lattice vector of the grating coupler, which can be expressed as

$$k_x^p = \frac{2\pi}{g}p \tag{22}$$

$$k_y^q = \frac{2\pi}{g}q \tag{23}$$

where $p, q = -\infty, \ldots, -2, -1, 0, 1, 2, \ldots, \infty$ and g is the period of the grating. The total wave vector of each order diffracted waves, including nonpropagating waves, obeys

$$(k_x^p)^2 + (k_y^q)^2 + (k_z^{pq})^2 = (2\pi/\lambda)^2 \tag{24}$$

where k_z^{pq} is the perpendicular wave vector of the diffracted waves which is real for propagating waves and pure imaginary for evanescent waves, and λ is the wavelength of the incident wave. For

back side illumination as shown in Fig.3.3.1(b), the wave solution in the quantum well side consists of the incident wave plus a superposition of reflected diffracted waves. The wave solution in the air region consists of a superposition of transmitted diffracted waves. The incident, reflected and transmitted waves are expressed, respectively, as following

$$\vec{E}^i = A_{001}\vec{\Phi}_{001} + A_{002}\vec{\Phi}_{002} \tag{25}$$

$$\vec{E}^r = \sum_{pq}\sum_{r=1}^{2} R_{pqr}\vec{\Phi}_{pqr} \tag{26}$$

$$\vec{E}^t = \sum_{pq}\sum_{r=1}^{2} T_{pqr}\vec{\Phi}_{pqr} \tag{27}$$

where $\vec{\Phi}_{pqr}$ are the orthonormal Floquet modes, A_{00r}, R_{pqr} and T_{pqr} are incident, reflected and transmitted coefficients, and $r = 1$ or 2 is designated as TE or TM Floquet modes, respectively. By matching the tangential electric field of each wave at the grating-air interface, the coefficients of the diffracted waves are obtained in terms of the power of incident wave. The normalized power carried by (p, q) order TM reflected waves is given by

$$\mathcal{P}_{pq2} = \frac{|R_{pq2}|^2}{\cos\theta_{pq2}} \tag{28}$$

where θ_{pq2} is the angle between the diffracted ray and the grating normal. Figure 3.3.2 shows the normalized power of the first order diffracted waves versus the wavelength for two sets of different grating parameters under back side illumination, where γ is the angle enclosed by the electric field vector of the diffracted waves and the free carrier moving vector $\hat{z}$ which is used to determine the absorption constant of the QWIP. The 2D square mesh metal grating coupled GaAs SBTM QWIP structure used in the present analysis is based on the bound ground state in the enlarged well to the global miniband in the superlattice. The detector layers consist of 20-period of $In_{0.03}Ga_{0.97}As$ quantum wells with a well width of $101\mathring{A}$ and a dopant density of 1.4×10^{18} cm^{-3}. The barrier layer on each side of the quantum well consists of a 5-period of undoped $Al_{0.4}Ga_{0.6}As(30\mathring{A})/GaAs(55\mathring{A})$ superlattice layers which were grown alternatively with the InGaAs quantum wells. The corresponding absorption constant α of the 2D grating coupled SBTM QWIP is shown in Fig.3.3.3.

In the measurement of photocurrent, a lock-in chopper technique is employed to enhance the signal and block out the noise for narrow band detection. This technique can greatly improve the sensitivity of the measurement system. In addition, a single grating monochromator is used to pass the monochromatic wavelength of the IR source. In order to eliminate the back-ground radiation,

the IR light source (globar) is modulated by a chopper at certain fraquency and the detected modulated signal is sent to the lock-in amplifier with the chopper's phase. The lock-in amplifier functions as both a phase sensitive detector and a narrow bandwidth amplifier which only amplifies the signal at chopper frequency and filters out the unmodulated signal. The bandwidth of the modulated signal depends on the chopper frequency and the size of incident beam. Higher frequency will narrow the detected bandwidth and lower the incident power accessing to the detector.

A bias voltage is required for the photoconductive operation QWIPs. In contrast, noise is the limitation of small signal detection in the applications of long wavelength QWIPs. For this reason, the bias circuit must be carefully designed in order not to introduce the excess noise. For the use of a TTL power supply, the noise current from the voltage source may be so large that dominates the total noise current. To solve this, we use the dry battery as voltage source because of its low noise level in comparison with that of a TTL power supply. To supply the desired bias voltage, an operational amplifier circuit including a variable resistance is employed with a LF356 an internally compensated low noise operation amplifier incorporated with highly matched JFET input stage. The JFETs circuit can enhance the input characteristics impedance ($R_i = 10^{12}\Omega$) and offer very high differential gain (DC voltage gain = 106dB). The bias voltage is fed into the noninvert input of the OP AMP through a voltage divider. Accordingly, the invert input will show up the same bias voltage as the noninvert input because of the virtual ground between both the OP AMP inputs. The SBTM QWIP mesa with area of $208\times208\mu m^2$ was created by chemical etching through the quantum well active layers and stopped at the 1-μm-thick GaAs buffer layer for ohmic contact. Subtracting the area of contact ring and bonding pad, the grating active area of the detector is 26,400 μm^2.

Figure 3.3.4 shows the responsivity of the grating coupled InGaAs SBTM QWIP with different grating periods and aperture sizes under different coupling scheme and with a bias voltage $V_b = -2.5$ V and T = 77 K. In this figure, the theoretical spectral responsivity R_I is calculated by substituting the coupling quantum efficiency into the following expression

$$R_I = \eta g_o \frac{\lambda}{1.24} \tag{29}$$

where the optical gain $g_o = 0.205$ is obtained from the noise gain measurements at 77 K under the assumption that these two gains are equal. According to our previous calculations, the responsivity of a SBTM QWIP under back side illumination is 2.34 times higher than that under front side illumination. This calculations are based on the assumptions that the impedance Z_{sub} looking from the detector substrate surface into the quantum well region is equal to $Z_0/3.25$ so that the

reflectivity at the detector substrate-air interface is equal to 0.28. However, using 2D square mesh metal grating on top of the SBTM QWIP changes Z_{sub} drastically. From the experimental results, an estimated reflectivity at the detector substrate-air interface is equal to 0.5, that is, 50% of the incident power will be reflected back to the air for a back side illumination with a 2D metal grating deposited on top surface of the SBTM QWIP.

In conclusion, we have performed a theoretical and experimental study of the coupling quantum efficiency and responsivity in a 2D square mesh metal grating coupled InGaAs SBTM QWIPs under different grating periods and aperture sizes. The maximum responsivity for an InGaAs SBTM QWIP was found to be 0.5 A/W with grating parameters $g = 3.3\mu$m and $a = 2\mu$m. The responsivity may be further improved by using grating parameters with $g = 2.9\mu$m and $a = 1.7\mu$m.

References

1. K. W. Goossen and S. A. Lyon, Appl. Phys. Lett. **47**, 1257 (1985).
2. R. J. Baüerle, T. Elsaesser, and W. Kaiser, Phys. Rev. B **38**, 4370 (1988).
3. K. M. S. V. Bandara. D. D. Coon, and Byungsung O, Appl. Phys. Lett. **53**, 1931 (1988).
4. M. J. Kane, M. T. Emeny, N. Apsley, C. R. Whitehouse and D. Lee, Semicond. Sci. Tech. **3**, 722 (1988).
5. B. F. Levine, C. G. Bethea, G. Hasnian, V. O. Shen, E. Pelve, and P. R.Abbott, Appl. Phys. Lett. **56**, 851 (1990).
6. S. D. Gunapala, B. F. Levine, D. Ritter, R. Hamm, and M. B. Panish, Appl. Phys. Lett. **58**, 2024 (1991).
7. L. C. West and S. J. Eglash, Appl. Phys. Lett. **46**, 1156 (1985).
8. S. J. Allen, Jr., D. C. Tsui, and B. Vinter, Solid State Commun. **20**, 425 (1976).
9. J. Y. Andersson, L. Lundqvist, and Z. F. Paska, Appl. Phys. Lett. **58**, 2264 (1991).
10. K. W. Goossen and S. A. Lyon, Appl. Phys. Lett. **53**, 1027 (1988).
11. W. J. Li, B. D. McCombe, F. A. Chamber, G. P. Devane,J. Ralston, and G. Wicks, Surf. Sci. **228**, 164 (1990).
12. J. Y. Andersson, L. Lundqvist, and Z. F. Paska, Appl. Phys. Lett. **59**, 857 (1991).
13. J. Y. Andersson and L. Lundqvist, J. Appl. Phys. **71**, 3600 (1992).
14. Y. C. Wang and S. S. Li, J. Appl. Phys., Aug. 15 (1993) (to be published).
15. L. S. Yu and S. S. Li, Appl. Phys. Lett. **59**, 1332 (1991).

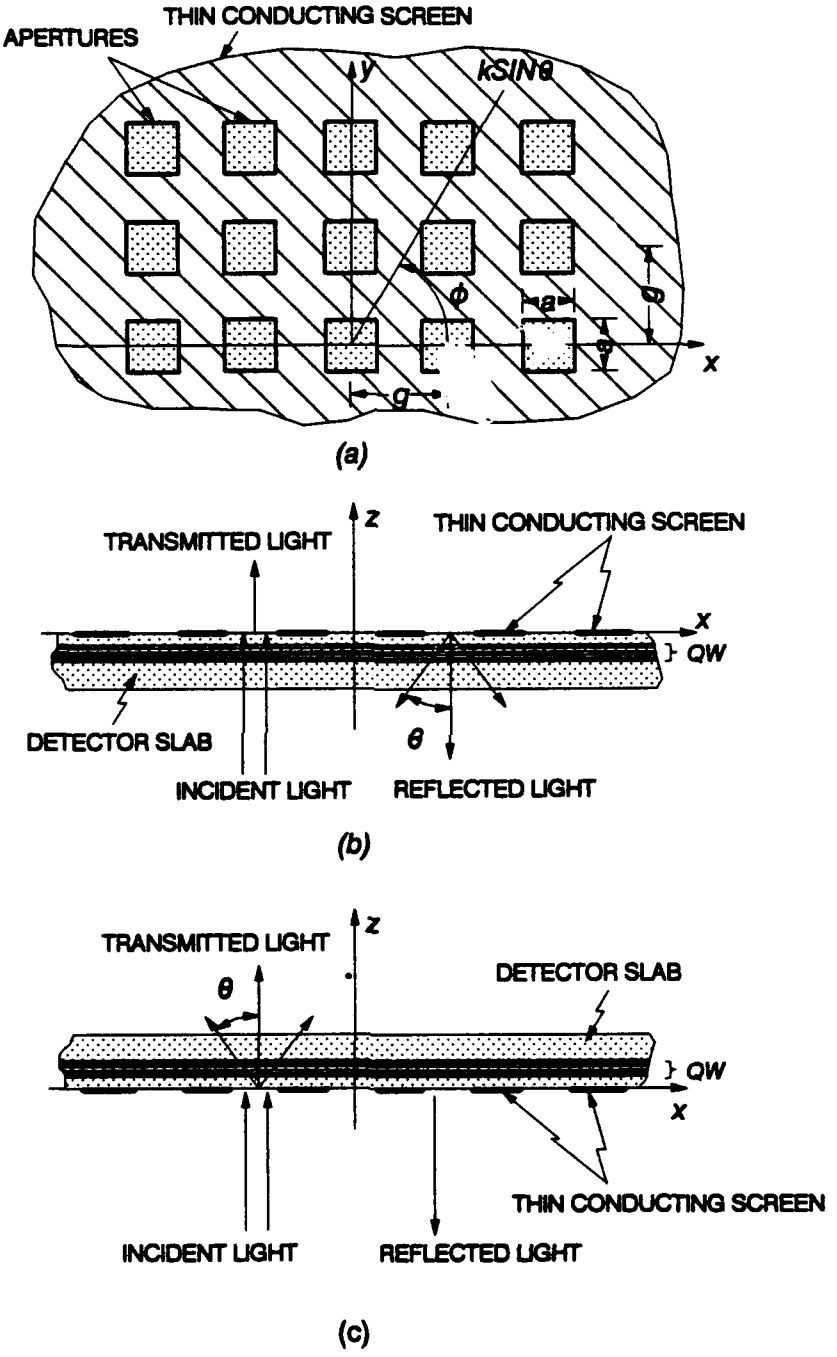

Figure 3.3.1 (a) Top view of a 2-D square mesh metal grating coupler, showing the grating period `g' and aperture size `a', (b) side view of backside normal incident illumination, and (c) front side illumination.

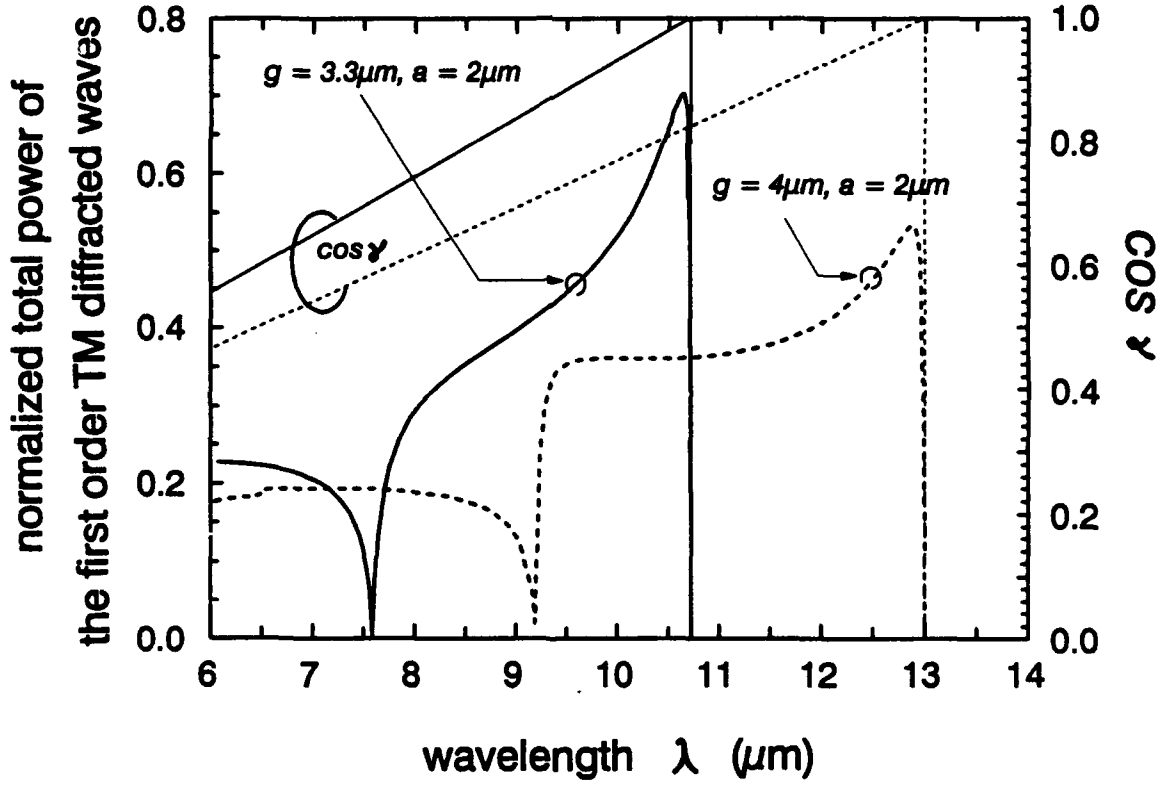

Figure 3.3.2 Simulation of the normalized total power of the first order TM diffracted waves and cosγ versus wavelength for two different grating periods and aperture sizes.

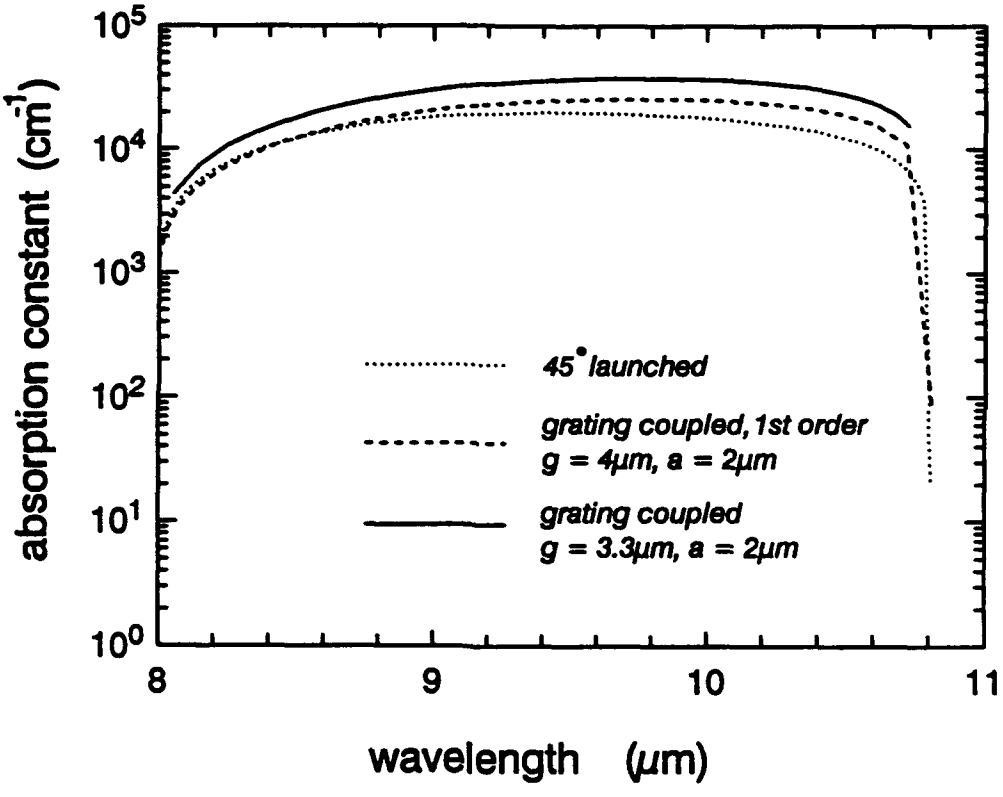

Figure 3.3.3 Calculated absorption coefficient versus wavelength for the InGaAs SBTM QWIP for 45 ° lunched and 2D square mesh grating coupler of different grating periods and aperture sizes.

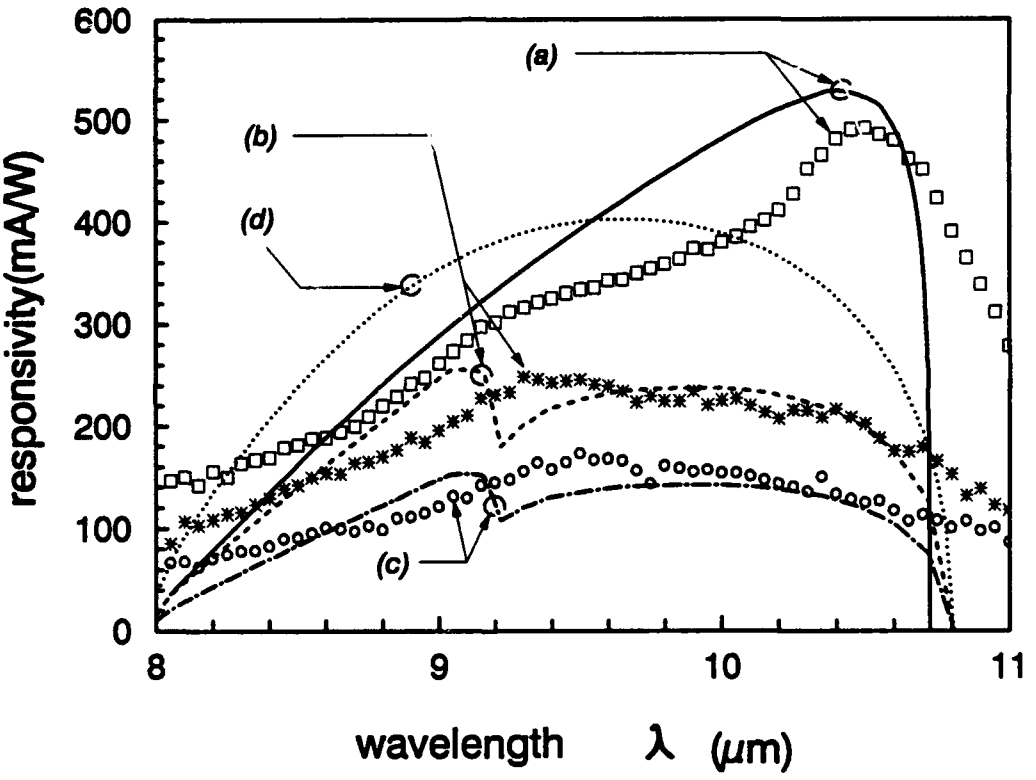

Figure 3.3.4 Calculated and measured responsivities for the InGaAs SBTM QWIP: (a) Under backside illumination, g = 3.3 um, a = 2 um, (b) backside illumination, g = 4 um, a = 2 um, (c) frontside illumination, g = 4 um, a = 2 um, and (d) illuminated at 45 ^{o} polished facet. The discrete points are the measured data.

3.4. Broadband Coupling of A Dual-Mode (DM) Operation GaAs QWIP Using A 2-D Square Mesh Metal Grating Coupler

Summary: Effecient coupling of infrared radiation into a dual-mode operation GaAs QWIP has been realized by using a planar 2-dimensional (2D) square mesh metal grating coupler formed on the top surface of this detector. A broad coupling bandwidth for such a grating structure is needed for coupling the mid-wavelength (3-5 μm) and long-wavelength (8-12 μm) infrared radiation into such a QWIP. A flat coupling quantum efficiency of $\eta = 18\%$ in the 6-8 μm and 10-13μm wavelength regimes was obtained for this grating coupled GaAs QWIP with grating period $g = 4\mu$m an aperture width $a = 2\mu$m.

3.4.1 Introduction

Long-wavelength intersubband transition quantum well infrared photodetectors (QWIPs) for detection in the 8-12μm atmospheric window have been extensively studied in recent years.[1,2] Most of the works on intersubband absorption have been based on the photoconductive (PC) mode detection.[3–5] However, studies of the photovoltaic (PV) mode detection QWIPs[6–8] have also been reported in the literature. In this section we report a grating coupled dual-mode (PC and PV) detection GaAs/AlGaAs QWIP based on the bound-to-continuum (BTC) states transition mechanism. The coupling quantum efficiency in such a QWIP can be greatly enhanced by using a 2D broad band planar metal grating coupler under backside normal incidence illumination.

The polarization selection rule for the intersubband absorption requires one component of the electric field vectors of the infrared (IR) radiation to be polarized perpendicular to the quantum well layer planes.[9] That is, the angle of interacting light with respect to the quantum well layers must be different from zero in order to induce intersubband absorption and to produce photocurrent. As a result, for practical applications such as focal plane arrays, it is necessary to fabricate a grating coupler on the top surface of the QWIP to scatter the normal incident IR radiation into an angle suitable for intersubband absorption. On the other hand, the peak response wavelengths for the PC and PV mode detection are occured in the MWIR (3-5 μm) and LWIR bands (8-12 μm), respectively, developing a broad band (covering 3-5 and 8-12 μm bands) grating coupler is highly desirable for coupling such a two-color detection QWIP. A wide variety of coupling techniques such as incorporating a one-dimensional lamellar grating coupler,[10,11] an etching formed 2D reflection cross grating coupler,[12] a planar 2D square mesh grating coupler or a prism coupler[13] on top of the detector sample have been reported for the QWIPs. More recently, we reported a 2D double

periodic square mesh metal grating coupler for the QWIPs which offers several advantages over other techniques. These include: (i) it effectively scatters the normal incident IR radiation into an absorbable angle independent of light polarization, (ii) it is capable of coupling a broad IR radiation spectrum, (iii) it is easy to fabricate by using a simpler planar structure to directly deposit the metal mesh onto the detector surface, as shown in Fig.3.4.1. In the grating design, the square aperture width 'a' and grating period 'g' are the two key parameters of major interest. It can be shown theoretically that the coupling of incident IR radiation power for such a grating structure is a function of the ratio of 'a' to 'g', which is called the 'strip factor'. For an effective broad band coupling, the strip factor ($= a/g$) of a 2D square mesh metal grating must fall between 0.5 and 0.63. Since the peak response wavelengths for the PC and PV mode detection are occured at $\lambda = 7.7\mu$m and 12 μm respectively, and the refractive index of GaAs is 3.25, the grating period for this QWIP is chosen to be 4μm to cover both the intersubband absorption bands.

The GaAs DM-QWIP structure used in this study was grown by the molecular beam epitaxy (MBE) technique. A 1-μm-thick highly doped (2×10^{18} cm^{-3}) n$^+$-GaAs bottom contact layer was first grown on a lattice matched semi-insulating GaAs substrate. This is followed by the growth of 40 periods of enlarged GaAs quantum wells with a well width of 110$\AA$ and a dopant density of 5×10^{18} cm^{-3}. The enlarged barrier layers on each side of the quantum well consist of an undoped $Al_{0.25}Ga_{0.75}As$ layer with a barrier width of 875$\AA$. Finally, a highly doped (2×10^{18} cm^{-3}) n$^+$-GaAs cap layer of 0.45μm thick was grown on top of the QWIP to complete the structure and facilitate ohmic contacts. The physical parameters of the QWIP are chosen so that there are two bound states (i.e., E_{w0} and E_{w1}) inside the enlarged well, and the continuum states (E_{cn}) are just slightly above the top of the barrier layer. A high dopant concentration of 5×10^{18} cm^{-3} was used in the enlarged GaAs quantum well so that the ground state E_{w0} and the first excited state E_{w1} are heavily populated by the electrons to enhance absorption of infrared radiation in the quantum well. In order to minimize the undesirable tunneling current through the barrier layers, a thick (875 Å) undoped $Al_{0.25}Ga_{0.75}As$ barrier layer was used in this QWIP to suppress the undesired tunneling current from the heavily populated ground state E_{w0} and the first excited state E_{w1} in the quantum well.

The DM-QWIP mesas of 200×200 μm^2 active area were formed by chemical etching through the active layers down to the 1-μm-thick bottom contact layer. A square contact ring composed of AuGe/Ni/Au materials was first deposited around the periphery of the mesa and alloyed for ohmic contact formation. The metal grating was then deposited within the interior of the contact ring by

using electron beam (e-beam) evaporation of Au followed by lift-off process.

3.4.2 Theory

Theoretical calculations of the energy levels in the QWIP were carried out by using the multi-layer transfer matrix method, and results yielded $E_{w0} = 23\text{meV}$, $E_{w1} = 90\text{meV}$ and $E_{cn} \geq 188\text{meV}$, where the energy is measured from the bottom of conduction band of GaAs quantum well. The two intersubband transitions corresponding to the infrared wavelengths of 7.2 and 12 μm were observed in this QWIP. The first transition is from the localized ground-state E_{w0} in the GaAs quantum well to the continuum band states E_{cn} above the AlGaAs barrier layer. The second transition is taken place from the first excited state E_{w1} to the continuum states E_{cn}. Furthermore, the asymmetrical energy band bending due to doping impurity migration and heavy doping effects lead to the creation of internal photovoltage (i.e., Dember voltage) under illumination.

To design a broad band grating coupler with high coupling quantum efficiency, we performed the numerical analysis of a planar 2D square mesh metal grating coupler. Figure 3.4.1 shows the layout of a 2D square mesh metal grating coupler formed on the top surface of a GaAs DM-QWIP, where $a = 2\mu$m is the square aperture width and $g = 4\mu$m is the grating period. The IR radiation is incident normally on the substrate of the grating coupled QWIP. The square apertures of the grating are arranged along two orthogonal coordinates $\hat{x}$ and $\hat{y}$ making the whole grating structure as equal spaced parallel metal lines intersect one another at rectangular angle. The unknown electromagnetic (EM) waves near the grating are modeled by using modal expansion method[15]. Taking wave theory in periodical structure into consideration, the transverse vector field of incident, reflected and transmitted waves are expressed as sums of Floquet modes $\vec{\Phi}_{pqr}$, where (p, q) is the diffracted order, $r = 1, 2$ denotes the TE and TM Floquet modes, respectively. Employing the method of moments by expanding the EM waves within the square aperture as a superposition of waveguide modes, a matrix expression can be derived as follows:

$$\left[Y_m^M\right] [W_m] = [I_m] \tag{30}$$

where

$$Y_m^M = \sum_{pq} \sum_{r=1}^{2} \left(\frac{1}{\eta_{pqr}} + \frac{1}{\eta_{pqr}^d}\right) C_{pqr}^{M*} C_{pqr}^m$$

$$C_{pqr}^m = \int\int_{-a/2 \leq x,y \leq a/2} \vec{\Phi}_{pqr}^* \cdot \vec{\Pi}_m dx dy \tag{31}$$

and incident dependent matrix

$$I_m = 2 \cdot \sum_{r=1}^{2} A_{00r} \frac{1}{\eta^d_{00r}} C^{m*}_{00r} \tag{32}$$

The $\vec{\Pi}_m$ are the waveguide modes spanned by the square aperture, W_m represents the corresponding expansion coefficient, η_{pqr} and η^d_{pqr} are the impedances of the Floquet modes on the two sides of the mesh grating, and A_{00r} are the expansion coefficients of the incident field. The integrals C^m_{pqr} and the elements of Y^M_m are complex numbers. The absorption constant[14] α of a QWIP depends on $\cos^2\gamma$, where γ is the angle between the electric field vector of the diffracted waves and the free carrier motion vector $\hat{z}$. For this reason, only TM propagating Floquet modes of the grating scattered field result in photo-response.[11] Besides, a larger value of $\cos^2\gamma$ implies a larger absorption constant. The cosine of the angle γ is given by

$$\cos\gamma_{pq2} = \frac{\lambda/n_r}{g} \cdot \sqrt{p^2+q^2} \tag{33}$$

where n_r is the refractive index of the medium in which the wave propagates, and the third subscript 2 represents TM Floquet modes. The quantum efficiency of the grating coupled QWIP depends not only on γ but also on the power of higher order TM propagating modes, which can be expressed as

$$\eta = \sum_i \mathcal{P}_i \cdot (1 - e^{-\alpha_i \cdot l}) \tag{34}$$

where $\mathcal{P}_i$ is the normalized power of the ith order propagating TM mode, α_i is the corresponding absorption constant, and l is the total length of doped quantum wells; in present case $l = (110\mathring{A}) \times$ (40 periods) $= 4400\mathring{A}$. After the inversion of matrix Y^M_m, the relative power and angle γ of the first two order diffracted waves as a function of wavelength λ are plotted in Fig.3.4.2, where cosine of the angle γ_i is the quantity used to calculate the absorption constant α_i of the ith order diffracted waves. The second order diffracted waves begin to propagate when λ is smaller than 9.19μm. By substituting the diffracted power $\mathcal{P}_i$ given in Fig.3.4.2 and the corresponding α_i into Eq.(5), the coupling quantum efficiency for the DM-QWIP can be readily calculated.

3.4.3 Results and Discussion

The photocurrent measurements were performed using a globar source, a ORIEL 77250 single grating monochromator, a current preamplifier and a programmed chopped lock-in amplifier combination. The sample was mounted in the cold head of a liquid helium closed-cycle cryogenic system. From the photocurrent measurement, together with the measurement of calibrated intensity at the sample position using a pyroelectric detector, the absolute spectral responsivity R_I for the QWIP

is shown in Fig.3.4.3 for a bias voltage $V_{bias} = 2V$ and temperature $T = 60$ K. The photocurrent under PV mode operation was measured by direct feeding the signals into the lock-in amplifier. Obviously, the performance of the DM-QWIP under PV mode operation is somewhat inferior to that under the PC mode operation. The intensity of the IR light source was suppressed by a band-pass filter in the short wavelength, as a result, the measured photocurrent of the detector becomes noisier. By considering not only the coupling efficiency but also the coupling uniformity over both the absorption bands of 6-8μm and 10-13μm, our theoretical analysis reveals that $g = 4\mu$m and $a/g = 0.5$ is the optimum grating dimension and period for this GaAs DM-QWIP. The coupling quantum efficiency of the DM-QWIP shown in Fig.3.4.4 was calculated by substituting the current responsivity into the following equation

$$\eta = \frac{R_I}{g_o \lambda} \cdot 1.24 \tag{35}$$

where the optical gain $g_o = 0.3$ is estimated from the measured noise spectrum at 77 K. Operation at a lower bias voltage is recommended for reducing the dark current. A flat coupling quantum efficiency of $\eta = 18\%$ over both the MWIR and LWIR absorption bands was obtained for this 2D square mesh metal grating coupler.

In conclusion, we have designed a broad band 2D square mesh metal grating coupler with good coupling quantum efficiency for the GaAs DM-QWIP. A measured responsivity of 0.27 A/W over wavelengths of 6.5 to 7.8μm and of 0.47 A/W over the wavelengths of 10.5 to 13μm were obtained for this planar 2D square mesh metal grating coupled DM-QWIP using grating parameters $g = 4\mu$m and $a = 2\mu$m. By using the 2D broad band grating coupler described in this section for normal incident illumination, the GaAs DM-QWIP reported here can be used for the MWIR and LWIR two-color staring focal plane arrays and infrared image sensor applications.

References

1. B. F. Levine, K. K. Choi, C. G. Bethea, J. Walker, and R. J. Malik, Appl. Phys. Lett. **50**, 1092 (1987).
2. K. M. S. V. Bandara, J.-W. Choe, and M. H. Francombe, Appl. Phys. Lett. **60**, 3022 (1992).
3. B. F. Levine, C. G. Bethea, G. Hasnian, V. O. Shen, E. Pelve, and P. R. Abbott, Appl. Phys. Lett. **56**, 851 (1990).
4. L. S. Yu and S. S. Li, Appl. Phys. Lett. **59**, 1332 (1991).
5. D. D. Coon, R. P. G. Karunasiri, and L. Z. Liu, Appl. Phys. Lett. **47**, 289 (1985).
6. A. Kastalsky, T. Duffield, S. J. Allen, and J. Harbison, Appl. Phys. Lett. **52**, 1320 (1988).
7. Y. H. Wang, S. S. Li, and P. Ho, Appl. Phys. Lett. **62**, 621 (1993).
8. C. S. Wu, C. P. Wen, R. N. Sato, M. Hu, C. W. Tu, J. Zhang L. D. Flesner, L. Pham, and P. S. Nayer, IEEE Trans. **ED-39** 234 (1992).
9. L. C. West and S. J. Eglash, Appl. Phys. Lett. **46**, 1156 (1985).
10. J. Y. Andersson, L. Lundqvist, and Z. F. Paska, Appl. Phys. Lett. **58**, 2264 (1991).
11. K. W. Goossen and S. A. Lyon, Appl. Phys. Lett. **47**, 1257 (1985).
12. J. Y. Andersson, L. Lundqvist, and Z. F. Paska, Appl. Phys. Lett. **59**, 857 (1991).
13. B. D. McCombe, R. T. Holm, and D. E. Schafer, Solid State Commun. **32**, 603 (1979).
14. Z. Ikonić, V. Milanović, and D. Tjapkin, Appl. Phys. Lett. **54**, 247 (1989).
15. C. C. Chen, IEEE MTT-**18**, 627 (1970).

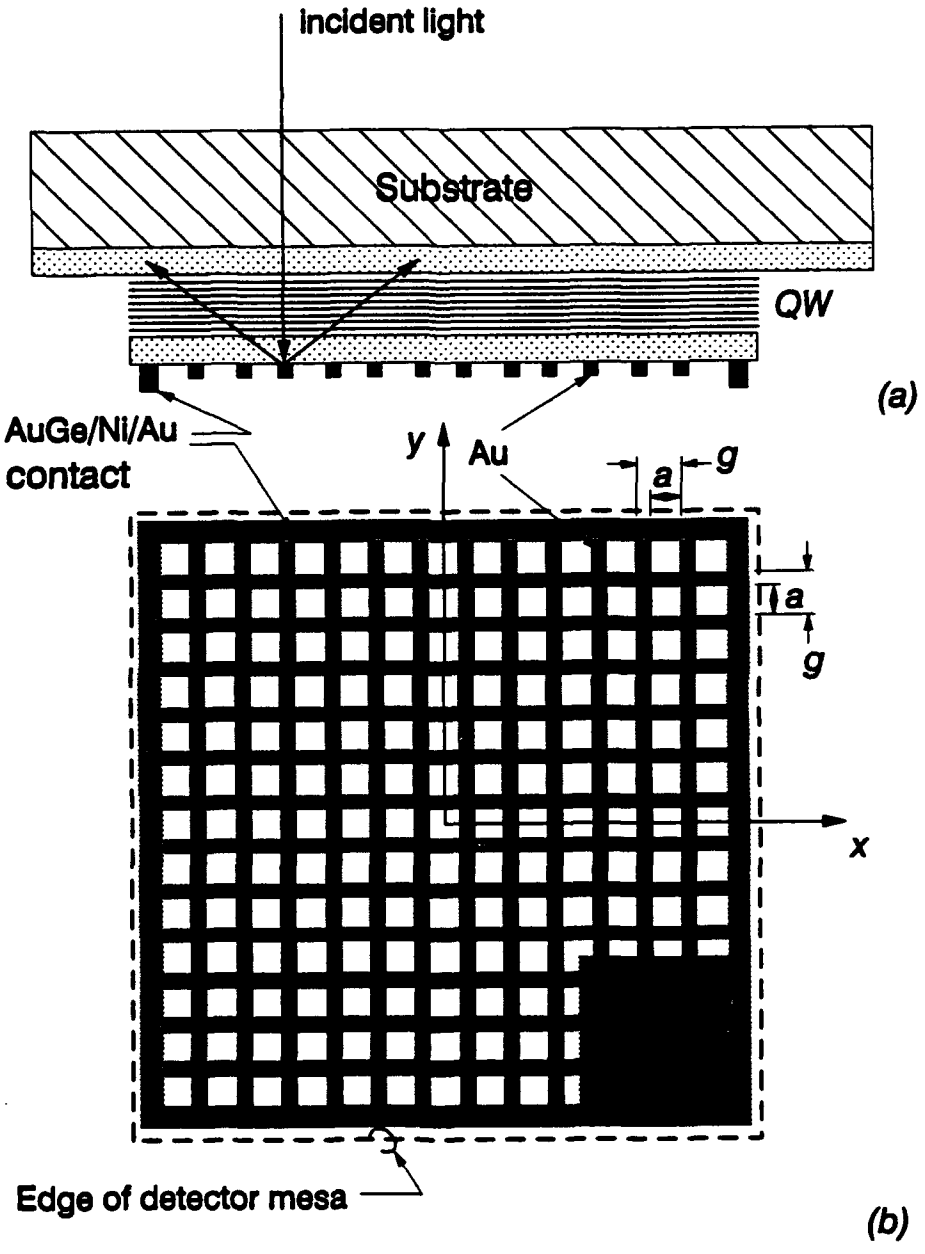

Figure 3.4. 1 (a) Cross sectional view of a 2D planar grating coupled GaAs/AlGaAs DM-QWIP, showing the back illumination at normal incidence.
(b) Top view of the 2D square mesh grating coupler ,showing the grating period and dimensions of grating aperture.

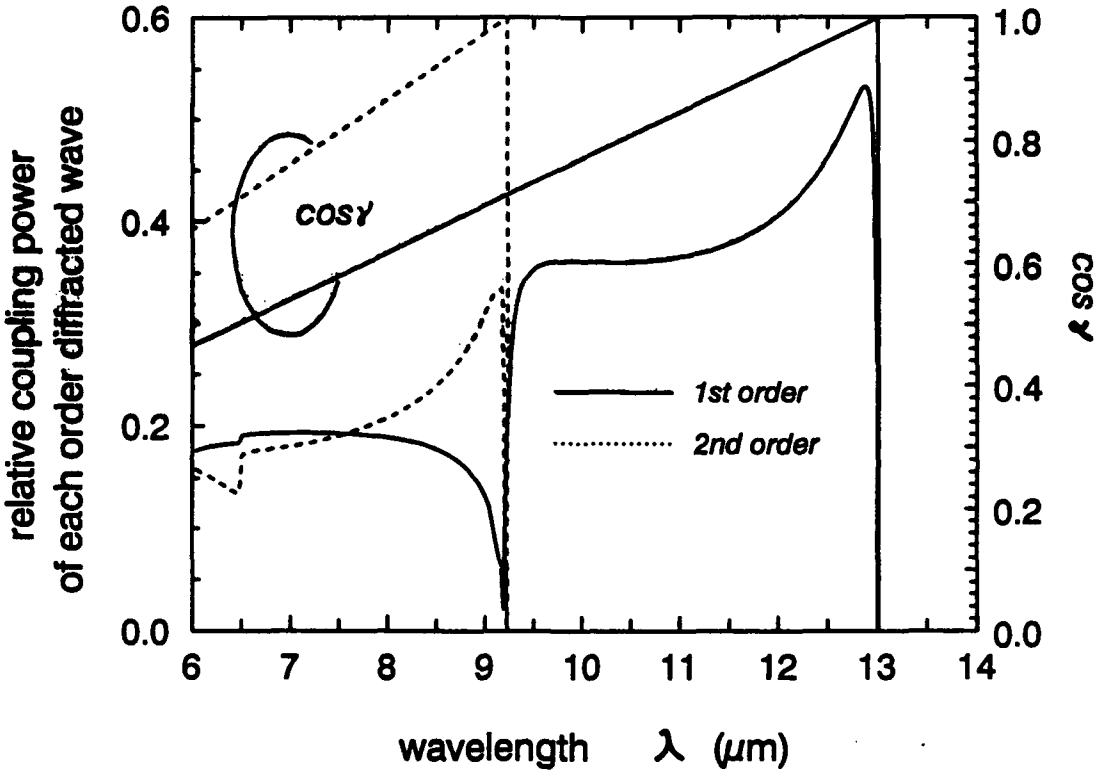

Figure 3.4.2 The simulated relative coupling power of the first and second order diffracted waves and the cos γ versus wavelength for a square mesh metal grating coupler with a grating parameters g=4 μm and a= 2.5 μm. Dashed line is for the 2nd order diffracted waves, and solid line is for the Ist. order diffracted waves.

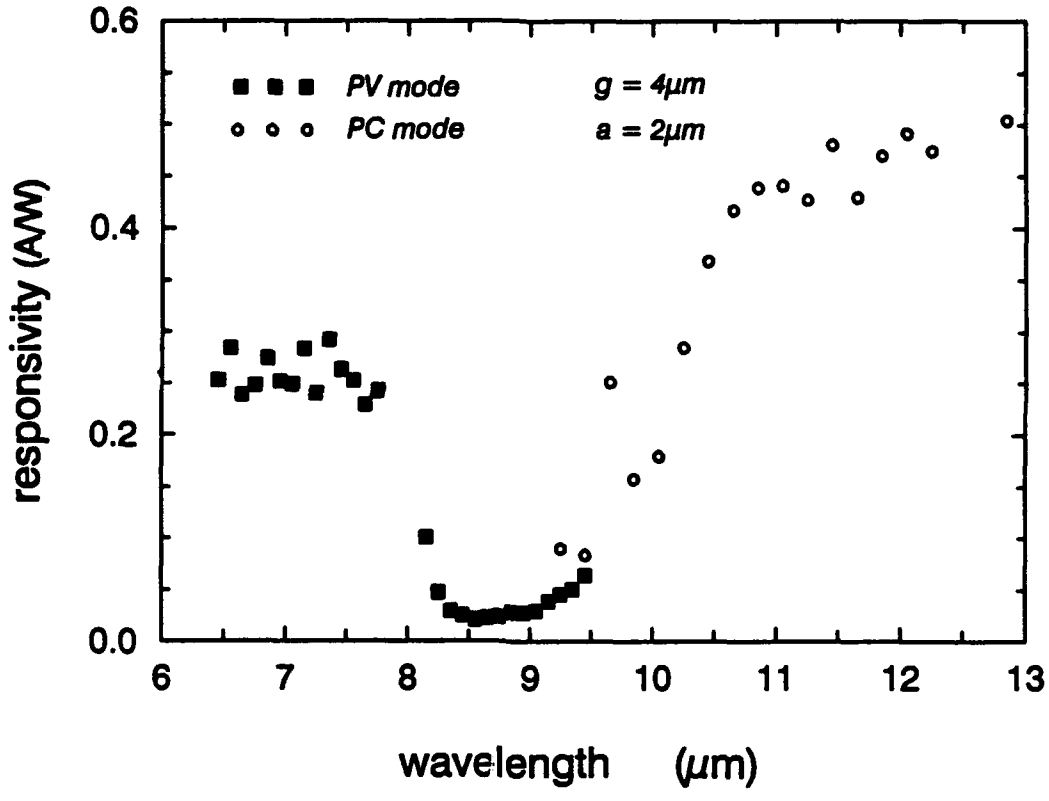

Figure 3.4.3 The measured PC and PV spectral responsivities for the grating coupled GaAs DM-QWIP, with g=4 um and a=2 um.

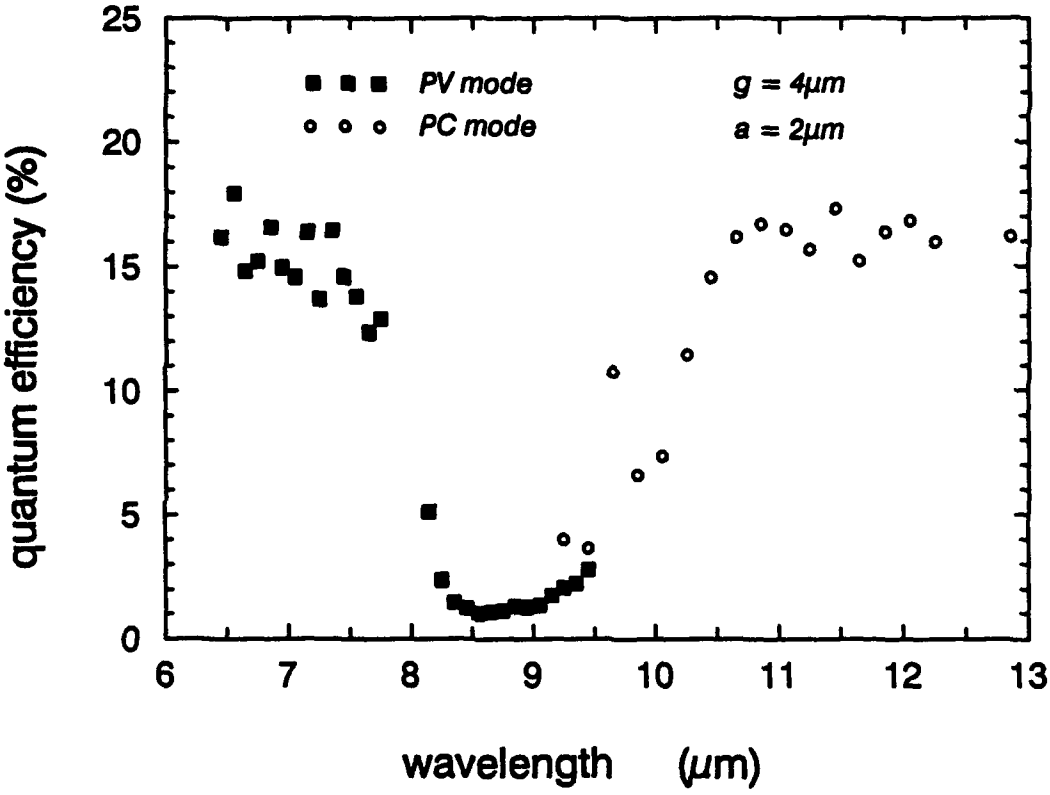

Figure 3.4. 4 The coupling quantum efficiency versus wavelength for the 2D square mesh grating coupled GaAs DM-QWIP.

3.5 Noise Characterization of III-V QWIPs

Summary: Dark current noise measurements between 10 and 10^5 Hz were carried out on four different III-V QWIPs designed for 8-12μm infrared (IR) detection at T = 77 K. Three devices (A, B, and C) with superlattice barriers are miniband QWIPs. The one with bulk barriers is a modified conventional GaAs QWIP with an enlarged GaAs quantum well and a thick bulk AlGaAs barrier layer. For frequencies between 10^2 and 10^4 Hz, the noise plateau levels stemming from the trapping and detrapping of electrons in the quantum wells were observed in QWIPs with superlattice barriers. From the measured noise data, the bias dependent noise gain and electron trapping probability were calculated. The device with bulk barriers only showed frequency dependent excess noise, most likely associated with interface state trapping at the GaAs/AlGaAs interfaces.

3.5.1 Basic Noise Theory

The most important sources of noise in solid-state devices are thermal noise, generation-recombination (g-r) noise, and flicker noise. The thermal noise of a device is caused by the random motion of the charge carriers. It produces a fluctuating emf across its terminals and is related to the device temperature. In semiconductors, the number of carriers fluctuate because of generation and recombination via donors, traps, recombination centers, or band-to-band transitions. Therefore, the resistance, R, fluctuates. If $\delta R(t)$ represents this fluctuation and a dc current I flows through the sample, then a fluctuating emf $\delta V(t) = I\delta R(t)$ will be developed across the terminals. This noise is called the generation-recombination noise, or g-r noise. Most of the noise sources has a frequency-independent spectrum at low frequencies, whereas the spectral intensity decreases at higher frequencies. The only exception is flicker noise, which usually has a $1/f$ spectrum throughout the entire frequency range. As a result, the flicker noise is often called $1/f$ noise. We shall briefly discuss each of these noise sources as follows.

(i) Thermal Noise:

Thermal noise was first discussed in detail by Nyquist in 1928[1]. Considering a frequency range extending from ν to $\nu + d\nu$ cycles per second and with a frequency interval of $d\nu$, the thermal electromotive force in a conductor of pure resistance R and of temperature T is given by

$$E^2 d\nu = 4RkTd\nu \tag{36}$$

From the Nyquist expression, the current spectral density of a resistor with resistance R is

$$S_i(f) = \frac{4kT}{R} \tag{37}$$

Thermal noise, also known as Johnson noise, is the dominant noise source at very low bias voltage in the miniband QWIPs.

(ii) Generation-Recombination (g-r) Noise:

The general equation for the fluctuation of free carrier density N in a solid is given by

$$\frac{dN}{dt} = g(N) - r(N) + \Delta g(t) - \Delta r(t) \tag{38}$$

where $g(N)$ and $r(N)$ denote the generation and recombination rates of carriers, respectively, and both are functions of N; $\Delta g(t)$ and $\Delta r(t)$ describe the randomness in these rates. With $N = N_o + \Delta N$ and the equilibrium condition $g(N_0) = r(N_0)$, the linearized Langevin differential equation is given by[2]

$$\frac{d\Delta N}{dt} = -\frac{\Delta N}{\tau} + \Delta g(t) - \Delta r(t) \tag{39}$$

where

$$\frac{1}{\tau} = \left(\frac{dr}{dN} - \frac{dg}{dN}\right)\Big|_{N_0}$$

Using Fourier analysis, the Langevin equation can be transformed into

$$S_N(f) = S_H(f)\frac{\tau^2}{1+\omega^2\tau^2} \tag{40}$$

where $\omega = 2\pi f$. By applying Milatz's theorem[3] and Poisson statistics, $\overline{\Delta N^2} = \overline{N}$, Eq. (5) can be written as

$$S_N(f) = 4\overline{\Delta N^2}\frac{\tau}{1+\omega^2\tau^2} \tag{41}$$

This equation is valid for all g-r processes described by fluctuations in a single variable N.

(iii) Flicker Noise:

Flicker noise is a very elusive noise source. It was discovered in vacuum tubes by Johnson[4] in 1925 and interpreted by Schottky in 1926[5]. The main characteristic of flicker noise is that it has a $1/f^\alpha$ spectrum with α close to unity. For that reason, the flicker noise also refers to as the $1/f$ noise.

A popular explanation for the $1/f$ noise is the so called McWhorter model[6] which interprets the $1/f$ spectrum as a superposition of a large number of Lorentzian spectra $4A_i\tau_i/(1+\omega^2\tau_i^2)$.

Another possible explanation for the $1/f$ noise is given in terms of mobility fluctuations occurring by lattice scattering and Brehm strahlung. These mechanisms produce true $1/f$ noise, i.e. with a frequency slope of -1. Excellent reviews on these topics are given in references [7,8]. The observed excess QWIP noise at low frequencies does not exactly show a -1 frequency slope, and thus the McWhorter model is more likely to apply to QWIP devices.

3.5.2 Noise Gain and Electron Trapping Probability

(i) Noise Gain:

In a QWIP, the number of conduction electrons is equal to the total number of carriers excited from the ground state to the continuum or miniband states. With the average current $\overline{I} = N_c i_e$, the noise current spectral density can be expressed in terms of $S_N(f)$, which is given by

$$\begin{aligned} S_i(f) = i_e{}^2 S_N(f) &= 4 i_e{}^2 \overline{\Delta N^2} \frac{\tau}{1+\omega^2\tau^2} \\ &= 4\overline{I}^2 \frac{\overline{\Delta N^2}}{N_c{}^2} \frac{\tau}{1+\omega^2\tau^2} \end{aligned} \tag{42}$$

For a QWIP, which satisfies the Poisson statistics, the variance $\overline{\Delta N^2}$ is equal to N_c. Using $\overline{I} = \frac{qN_c}{\tau_d}$, we can further simplify Eq. (7) to

$$\begin{aligned} S_i(f) &= 4\overline{I}^2 \frac{1}{N_c} \frac{\tau}{1+\omega^2\tau^2} \\ &= 4q\overline{I} \frac{\frac{\tau}{\tau_d}}{1+\omega^2\tau^2} \\ &= 4q\overline{I}g \frac{1}{1+\omega^2\tau^2} \end{aligned} \tag{43}$$

where $g = \frac{\tau}{\tau_d}$ is defined as the"noise current gain" in a QWIP; τ is the carrier lifetime and τ_d is the carrier transit time across the QWIP. In most of the cases, $\omega\tau \ll 1$, the g-r noise current spectral density function can be simplified to

$$S_i(f) \approx 4q\overline{I}g \tag{44}$$

(i) Electron Trapping Probability:

To derive the electron trapping probability equation for the QWIPs, three assumptions are needed for our model: (a) the photon flux is independent of the position; (b) the dark current is limited by thermal effects and the interwell tunneling is neglected, and (c) the ohmic contacts in the QWIPs are perfect contacts.

Now consider a QWIP with N quantum wells, and p denotes the electron trapping probability for the excited carriers in the extended states to be trapped into the quantum well ground state. Thus, $(1-p)$ is the probability that electrons escape from the well region. If i_m represents the photocurrent at each barrier m, then we have[9]

$$i_{m+1} = (1-p)i_m + q\phi\eta'(1-p) \tag{45}$$

where η' is the quantum efficiency for one quantum well. For current at the $(N+1)$th barrier, we have

$$\begin{aligned} i_{N+1} &= (1-p)i_N + q\phi\eta'(1-p) \\ &= (1-p)^N i_1 + q\phi\eta'[(1-p)^N + \cdots + (1-p)^1] \end{aligned} \tag{46}$$

Using the current continuity that $i_1 = i_2 = \cdots = i_{N+1} = i_{photo}$ and the quantum efficiency $\eta \approx N\eta'$, we obtain

$$\begin{aligned} i_{photo} &= q\phi\eta'\frac{(1-p)}{p} \\ &= q\phi\eta\frac{(1-p)}{Np} \end{aligned} \tag{47}$$

$$\tag{48}$$

where the photocurrent gain, g, is given by

$$g = \frac{(1-p)}{Np} \tag{49}$$

Since the current gain in the quantum wells is independent of the excitation methods (i.e., by photons or phonons), the photocurrent gain given in Eq. (13) should be the same as the noise gain.

3.5.3 Noise Measurments

The device parameters for the QWIP structures used in noise measurements are summarized in Table. 3.5.1[10–12], where L_B denotes the total superlattice (SL) or bulk barrier width between the two adjacent active quantum wells (QW), and N_D is the doping concentration for the quantum wells. One important parameter entering in our noise expressions is the differential resistance of the QWIP. To find this parameter, we first measured the dark current of our QWIPs using a HP4145B parameter analyzer. In the dark current measurements, the QWIP was submerged into liquid nitrogen to maintain a 77 K lattice temperature.

The differential resistance of the QWIP was calculated by using the first term of a Newton-Gregory forward polynomial approximation[14],

$$f'(x) = \frac{f(x+h) - f(x-h)}{2h} \tag{50}$$

The interpolating interval constant, h, for QWIP B was chosen to be 0.02 V. For the rest of our QWIPs, the constant h was 0.01 V. Fig. 3.5.1a and 1b show the dark current and differential resistance versus bias voltage for the four QWIPs measured at T = 77 K.

3.5.4 Results and Discussion

In the experiment, different bias voltages were applied to our samples. The noise current density spectra were measured under different bias conditions, and the results are discussed as follows:

QWIP A: A typical noise density spectra of QWIP A are shown in Fig. 3.5.2a. It shows that a strong noise signal was pick up at low frequencies. At the intermediate frequency range, the noise spectral density is affected by the RC parasitic effects, but after corrections are made,frequency independent noise levels result. These noise plateaus are attributed to electron trapping and de-trapping in the quantum wells and are g-r noise in nature. When the reverse bias voltage was over -1.06 V and the forward bias greater than 0.104 V, the $1/f$ noise becomes the dominant noise source.

The noise plateau levels, S_i, are plotted as a function of bias voltage in Fig. 3.5.3. This plot displays thermal noise up to 0.1 V after which g-r noise becomes dominant. An arrow indicates current noise level calculated using the Nyquist expression

$$S_i = 4KT\frac{dI}{dV} \tag{51}$$

By manipulating the g-r noise expression in Eq. (9), we obtain

$$g = \frac{S_{i_{(g-r)}}}{4q\bar{I}} \tag{52}$$

where

$$S_{i_{(g-r)}} = S_i - S_{i_{(thermal)}}$$

Fig. 3.5.4 shows the plot of noise gain,g, versus applied bias voltage V where we chose $S_{i_{(thermal)}} = 2.0 \times 10^{-24} A^2/Hz$. This figure shows that the gain increases with increasing bias voltage.

Since the electron trapping probability,p, can be expressed in terms of the noise gain, Eq. (13) can be written as

$$p = \frac{1}{1+Ng} \tag{53}$$

With the help of the above equation and using the number of quantum wells $N = 20$, we calculate p as a function of bias voltage for this QWIP, and the result is shown in Fig. 3.5.5, which shows that the electron trapping probability p decreases with increasing bias voltage.

QWIP B: Although the transition mechanism of QWIP B and QWIP A are identical, the doping concentration in the quantum well of QWIP B was chosen much lower than QWIP A to achieve a lower dark current. Thus, the d.c. resistance and the differential resistance for this sample areq uite high. Due to the relatively high differential resistance, especially at low applied bias voltage, the noise measurements at very low bias voltage fall below the sensitivity limit of our setup.

A typical noise current density spectrum of QWIP B is plotted in Fig. 3.5.2a. The strong signal at low frequencies is attributed to pick up. Neglecting this signal in the spectrum, the noise level, S_i, was found independent of frequency. We plotted these noise plateaus as a function of applied bias voltage in Fig. 3.5.3. The arrow indicates the current noise level calculated from Eq. (15).

From the Nyquist expression, the thermal noise of QWIP B is $1.0 \times 10^{-27} A^2/Hz$. Using this value, the noise gain can be calculated from Eq. (16). The result shows that the noise gain is slightly increased with increasing applied voltage as indicated in Fig. 3.5.4.

Using the number of quantum wells as 30 and the noise gain from Fig. 3.5.4, we plot the trapping probability versus bias voltage for QWIP B, as shown in Fig. 3.5.5. It can be seen that the trapping probability decreases slightly with increasing applied bias voltage.

QWIP C: The ($In_{0.07}Ga_{0.93}As$) used in the quantum wells of QWIP C has a lower conduction band edge than the GaAs/AlGaAs QWIPs discussed above. The lightly strained InGaAs quantum well was designed to bring down the conduction band edge of the quantum wells below the conduction band edge of the superlattice barriers. The purpose of this design is to lower the dark current of the device. As a result, although the differential resistance of this QWIP is not as high as that of QWIP B, the device's noise signal for bias voltages less than 0.1 V is still below the detection limit of our setup. We performed noise measurements on this sample for forward bias voltages between 0.255 V to 1.19 V, and the reverse bias voltages between 0.267 V and 3.88 V.

Fig. 3.5.2b shows a typical noise density spectrum. We found that QWIP C displays the g-r noise characteristics up to a forward bias of 0.9 V and a reverse bias of 3.1 V after which $1/f$ noise becomes dominant. The noise level, S_i, can be calculated using the method presented in this section and the result is plotted in Fig. 3.5.3.

QWIP C: The thermal noise of QWIP C is about $5.3 \times 10^{-27} A^2/Hz$ and is roughly an order of magnitude smaller than the measured value, S_i. It is safely to assume $S_{i_{(g-r)}} \approx S_i$. Using this approximation and well number $N = 40$, the noise gain and trapping probability can be calculated as a function of applied bias voltage. This bias dependency is shown in Fig. 3.5.4 and Fig. 3.5.5. The noise gain increases with increasing bias voltage and saturation sets in for voltages greater than 3 V. The trapping probability decreases with increasing bias and reaches a minimum value, 0.1, above 2 V.

QWIP D: This QWIP is a conventional bound-to-continuum states transition GaAs/AlGaAs QWIP with an enlarged quantum well and barrier width. The purpose of measuring noise in this QWIP is to compare its noise characteristic with those of the miniband transport QWIPs. The measured voltage range is from 1.0 to 3.0 V for the forward bias and from -0.7 to -4.4 V for the reverse bias. Typical noise density spectra for this QWIP are shown in Fig. 3.5.2b.

The results show that the frequency dependent excess noise dominates over the entire frequency span for all bias voltages for QWIP D. No frequency independent g-r noise can be detected in this QWIP. We attribute this excess noise to electron trapping in the interface of bulk barrier states.

3.5.5 Conclusions

In this section, studies of noise sources in both the standard and miniband QWIPs have been carried out. Several conclusions can be drawn from our results.

- QWIP A shows that thermal noise is dominant under very low applied bias voltages. The low bias noise data of QWIPs B and C can not be measured due to their large differential resistances, but seem to approach Nyquist values asymptotically. At high applied bias, the $1/f$ noise dominated in QWIPs A, B, and C. From our studies, the thermal noise is the dominant noise source in the very low bias region. As the applied voltage increases, g-r noise becomes dominant. Upon further increasing the bias voltage, the $1/f$ noise becomes dominant.

- For QWIP D the $1/f$ noise always dominates at all bias voltages. The $1/f$ noise in this sample is attributed to the electron trapping in the bulk barrier trapping states.
- For a QWIP, $(1-p)$ represents the probability for an excited carrier to escape the well region. Fig. (5) shows that the trapping probability p decreases with increasing bias voltage. Quantum well barrier lowering due to the applied field will increase electron emission from the wells with increasing applied voltage. As a result, $(1-p)$ will also be increased. This is consistent with our observations.

From the results of this study, we conclude that noise in miniband transition QWIPs is inherently lower than a standard QWIP. The reason for this may be attributed to the fact that superlattice barrier layers eliminate the dislocations or line defects present in the bulk barriers, and thus reduces the excess frequency dependent noise associated with these defects.

References

1. H. Nyquist Phys. Rev. **32**, 110 (1928).
2. P. Langevin, Compt. Rend. **146**, 530 (1908).
3. Aldert van der Ziel, ***Noise in Solid State Devices and Circuits*** (Wiley-Interscience, New York, 1986).
4. J. B. Johnson, Phys. Rev. **26**, 71 (1925).
5. W. Schottky, Phys. Rev. **28**, 74 (1926).
6. A. L. McWhorter, $1/f$ ***Noise and Related Surface Effects in Germanium*** (Lincoln Lab. Rpt. No. 80, Boston, 1955).
7. F. N. Hooge, Phys. Lett. **A29**, 139 (1969).
8. C. M. Van Vliet, Solid-St. Electron. **34**, 1 (1991).
9. H. C. Liu, Appl. Phys. Lett. **61** 2703 (1992).
10. Larry S. Yu, Y. H. Wang, Sheng S. Li, and Pin Ho, Appl. Phys. Lett. **60**, 992 (1992).
11. Y. H. Wang, Sheng S. Li, and Pin Ho, Appl. Phys. Lett. **62**, 93 (1993).
12. Y. H. Wang, Sheng S. Li, and Pin Ho, Appl. Phys, Lett. **62**, 621 (1993)
13. C. F. Gerald and P. O. Wheatley, ***Applied Numerical Analysis***, 3rd edition (Addison-Wesley, 1984).

Table.3.5.1 Device parameters for the four QWIPs used in this study

QWIP	A	B	C	D
SL barrier	$In_{0.52}Al_{0.48}As$	$Al_{0.32}Ga_{0.68}As$	$Al_{0.4}Ga_{0.6}As$	Barrier*
Width (Å)	35	78	30	$Al_{0.25}Ga_{0.75}As$
SL well	$In_{0.53}Ga_{0.47}As$	GaAs	GaAs	
Width (Å)	50	26	59	
L_B (Å)	460	598	478	875
QW	$In_{0.53}Ga_{0.47}As$	GaAs	$In_{0.07}Ga_{0.93}As$	GaAs
Width (Å)	110	85	106	110
$N_D(10^{18}cm^{-3})$	0.5	0.4	1.4	5.0
Periods	20	30	40	40
Substrate	InP	GaAs	GaAs	GaAs
Mesa (μm^2)	1.92×10^5	4×10^4	4.9×10^4	4×10^4
Transition	BTM	BTM	SBTM	BTC

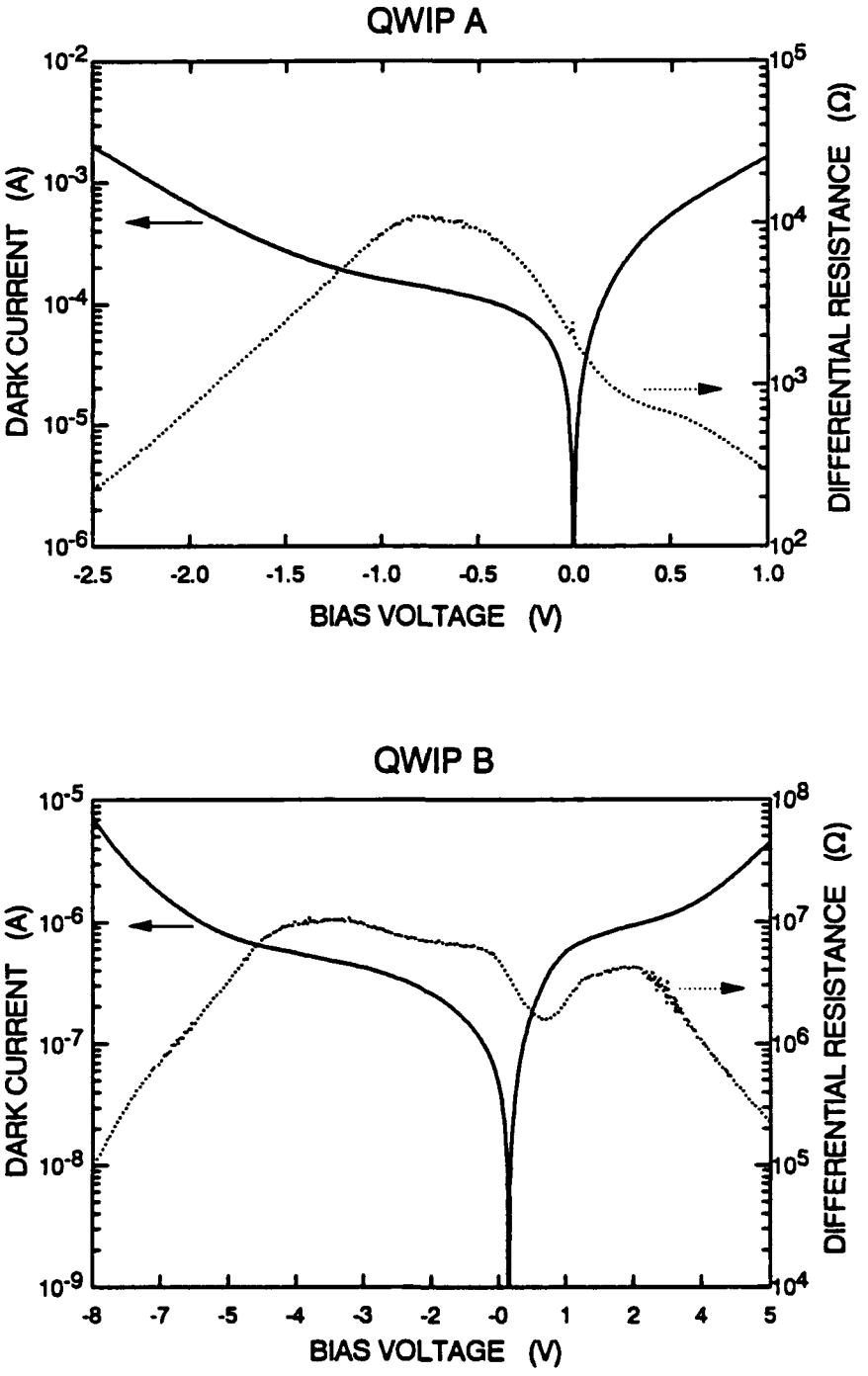

Figure 3.5.1a The dark current and differential resistance versus bias voltage for QWIP A and B measured at T = 77 K.

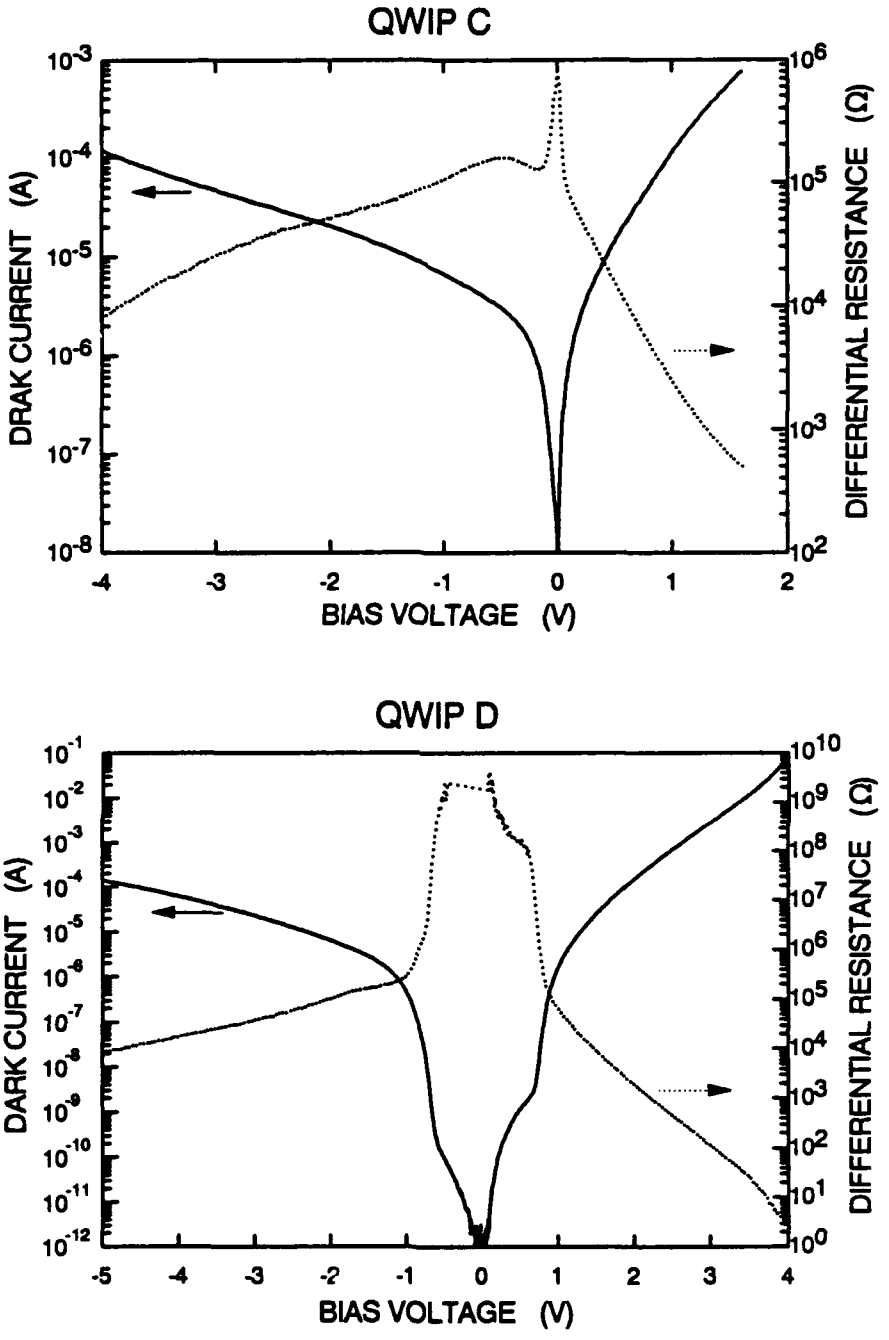

Figure 3.5.1b The dark current and differential resistance versus bias voltage for QWIP C and D measured at T = 77 K.

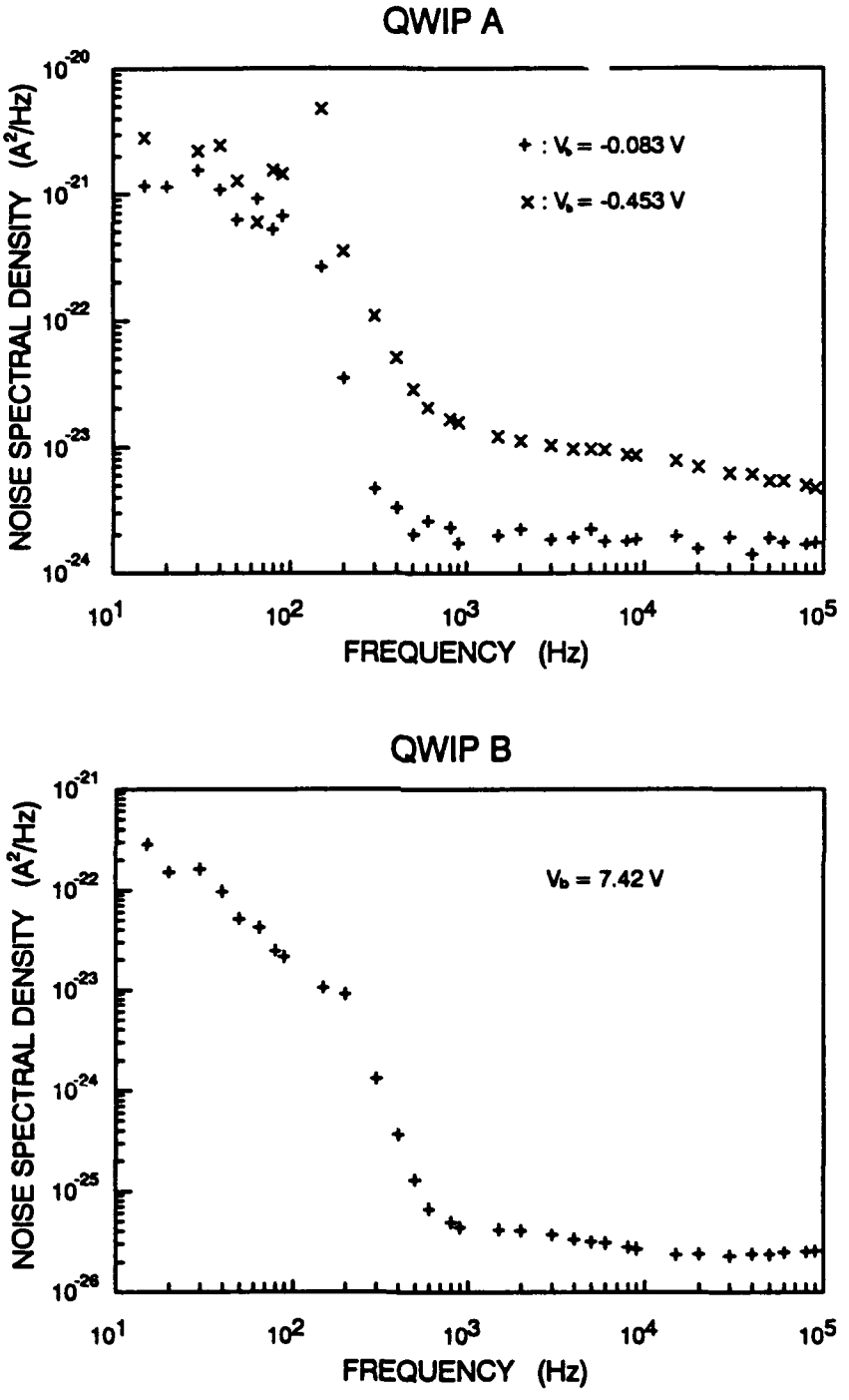

Figure 3.5.2a.The measured noise density versus frequency for QWIP A and B under different bias voltages.

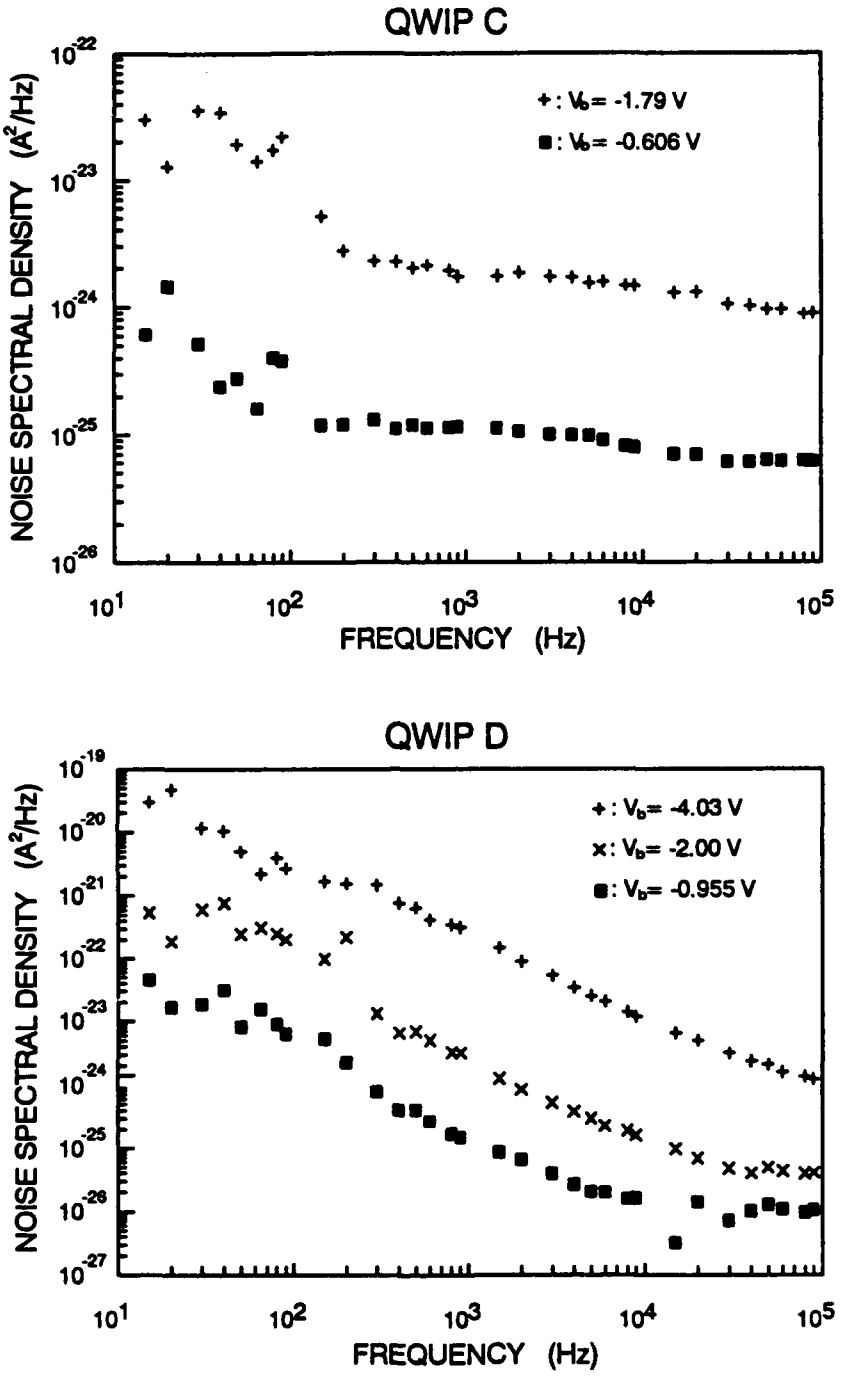

Figure 3.5.2b.The measured noise density versus frequency for QWIP C and D under different bias voltages.

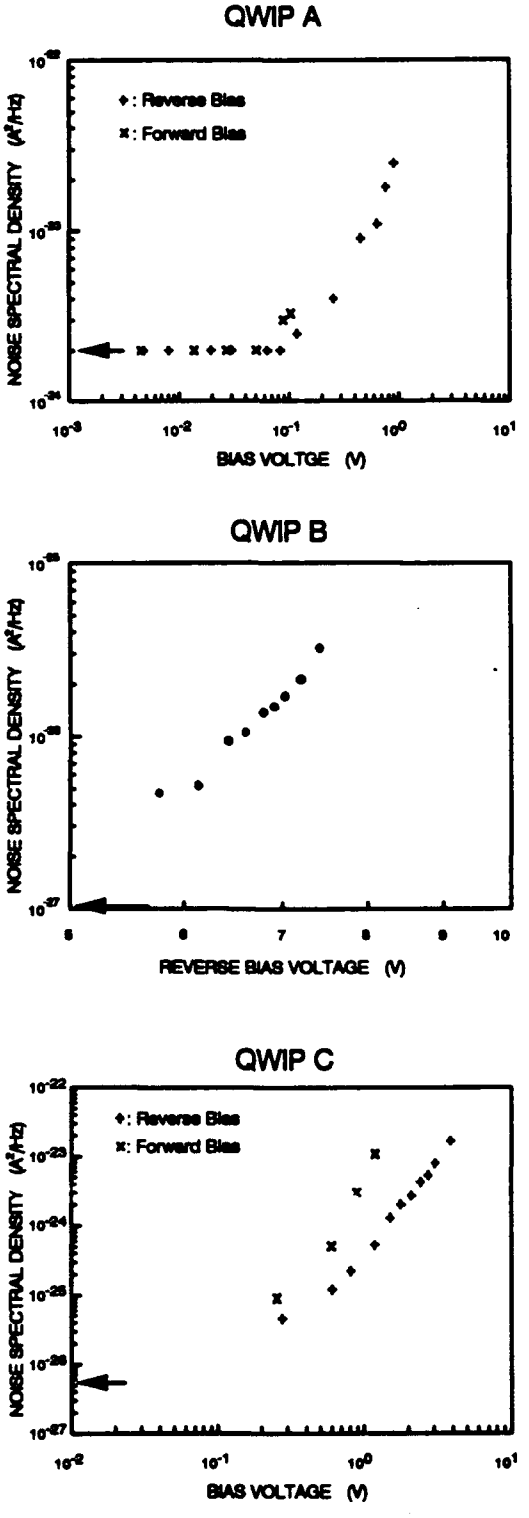

Figure 3.5.3 Noise spectral density versus bias voltage for QWIP A, B, and C under forward and reverse bias voltage.

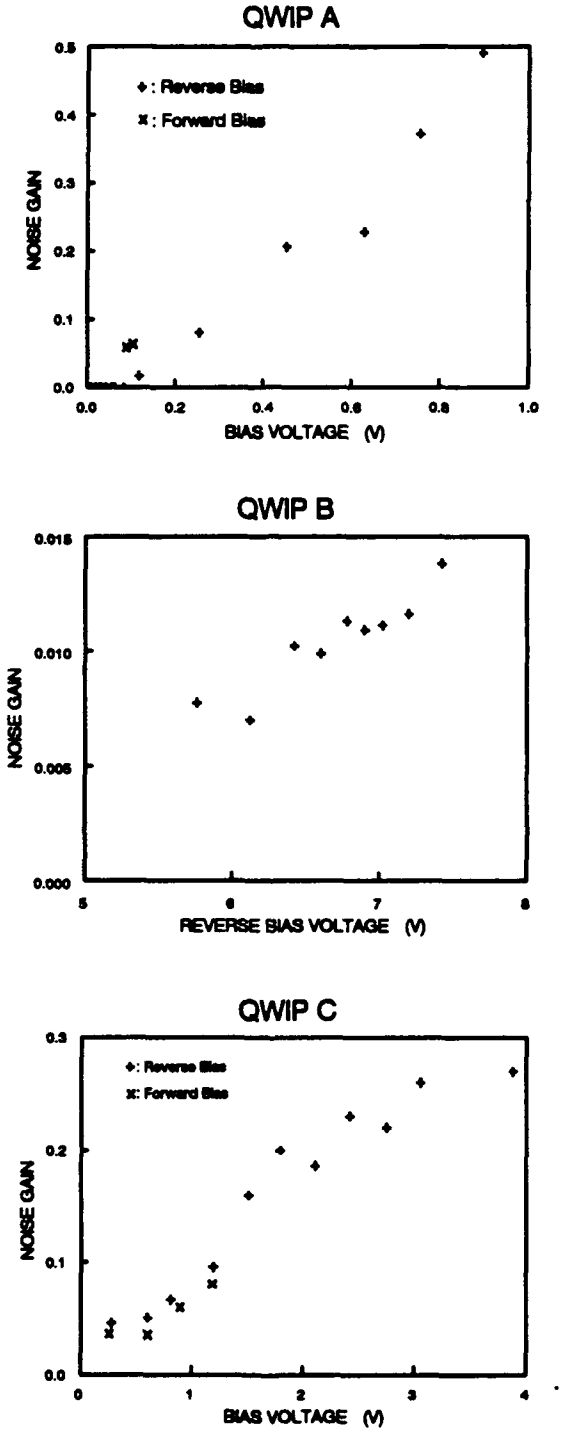

Figure 3.5.4 Noise gain versus bias voltage for QWIP A, B, and C under forward and reverse bias voltage.

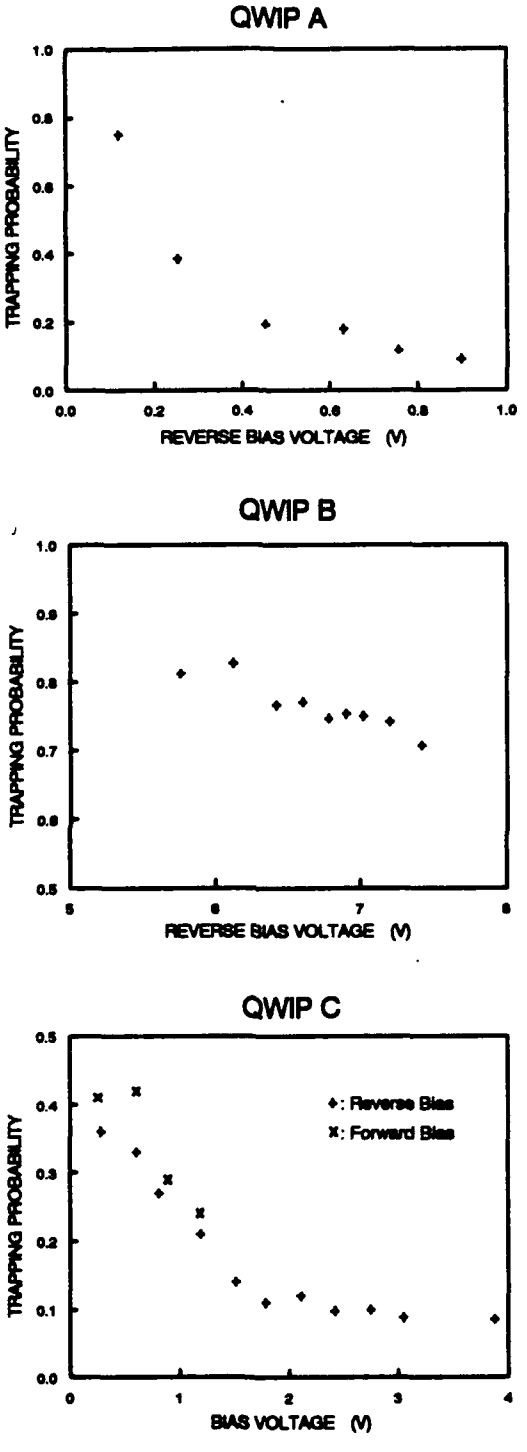

Figure 3.5.5 Electron trapping probability versus bias voltage for QWIP A, B, and C under forward and reverse bias voltage.